A critical appraisal of the sensitivity of detrital zircon U–Pb provenance data to constrain drainage network evolution in southeast Tibet

Shihu Li[1,2,*], Yani Najman[2], Pieter Vermeesch[3], Dan N. Barfod[4], Ian Millar[5], Andy Carter[3].

[1] State Key Laboratory of Lithospheric Evolution, Institute of Geology and Geophysics, Chinese Academy of Sciences, Beijing 100029, China

[2] Lancaster Environment Centre, Lancaster University, LA1 4YQ, Lancaster, UK

[3] Department of Earth Sciences, University College London, Gower Street, London WC1E 6BT, UK

[4] NEIF Argon Isotopes, University of Glasgow, SUERC, Glasgow, UK

[5] Geochronology and Tracers Facility, British Geological Survey, Keyworth, Nottingham NG12 5GG, UK

*Corresponding author at: State Key Laboratory of Lithospheric Evolution, Institute of Geology and Geophysics, Chinese Academy of Sciences, Beijing 100029, China

Email: lsh917@mail.iggcas.ac.cn

Abstract Provenance tools, particularly detrital zircon U–Pb analysis, have been widely employed to test drainage network evolution in southeast Tibet and its linkage with the growth of the Tibetan Plateau. Numerous provenance studies have been conducted on the sediments in the paleo-Yangtze and paleo-Red River drainage basins. Nevertheless, it is still hotly debated as to whether a “Mississippi” (dendritic) pattern Greater paleo-Red River, originating from southeast Tibet and draining to the South China Sea, existed in the early Cenozoic, and was subsequently captured by the paleo-lower Yangtze due to uplift of southeastern Tibet. In this study, in addition to presenting new data from the Gonjo and Jianchuan basins along which the Greater paleo-Red River is proposed to have flowed, we compiled all the published detrital zircon U–Pb data from the paleo-upper Yangtze and paleo-Red River drainage basins from Triassic and younger rocks. Our large database of detrital zircon U–Pb analyses shows that the different terranes in the paleo-upper Yangtze and paleo-Red River drainage basins have similar zircon U–Pb signatures since the Late Triassic closure of the Paleo-Tethys Ocean. Therefore, most of the sediments in the Cenozoic sedimentary basins in southeast Tibet could have been either deposited by long-distance transport in large rivers from southeast Tibet, or recycled from local bedrocks. Given the potential importance of sedimentary recycling that we have demonstrated, this poses challenges to the use of detrital zircon U–Pb analyses to determine paleodrainage in this region. We therefore further explored the previously relatively limited use of Sr–Nd isotopes on mudstones and detrital mica $^{40}Ar/^{39}Ar$ ages, with new analyses from the Gonjo and Jianchuan Basins, to determine if these techniques were better suited to reconstruct paleodrainage evolution. Whilst these techniques do show some promise, more analyses and strategic sampling are required to obtain a full understanding of the extent of their potential utility. Overall, our integrated provenance study indicates that the available data are not sufficiently conclusive to support or refute the Greater paleo-Red River capture model.

Keywords: Detrital zircon U–Pb, River capture, southeast Tibetan Plateau, Yangtze/Red River, Jianchuan and Gonjo basins.

Plain Language Summary (PLS) In the southeast margin of Tibetan Plateau, five large-scale rivers (Yangtze, Mekong, Salween, Irrawaddy, and Yarlung-Brahmaputra) flow through central Tibet to southeast Asia. How these rivers evolved during the Cenozoic uplift of the Tibetan Plateau remains a controversial issue. It has been hypothesized that, in the early Cenozoic, all the upper reaches of the five rivers flowed to the south and connected to the Red River flowing to the South China Sea, forming a "Mississippi" pattern Greater paleo-Red River; this Greater paleo-Red River was later captured by the lower Yangtze due to uplift of the Tibetan Plateau. Here we test the Greater paleo-Red River model by adding new data from Cenozoic sedimentary basins and providing a comprehensive compilation of available detrital zircon U-Pb data from different terranes of southeast Tibet. With this large dataset, we found that the source signatures for the various terranes from southeast Tibet are indistinguishable due to zircon recycling. Moreover, we explored the use of Sr–Nd isotopes and detrital mica $^{40}Ar/^{39}Ar$ ages as potential alternative provenance tools to test the river capture model. The overall provenance data are insufficient to test the validity of the Greater paleo-Red River capture model.

1. Introduction

Tectonic uplift, climate change, river erosion, and alluvial deposition are fundamental processes that have acted to shape the present landscape. Fluvial systems respond rapidly to climate change and/or tectonic events, as reflected in lateral channel shifting, headward erosion, ridge migration, and river captures, which are major influences on the development of the topography we see today. Therefore, deciphering paleodrainage network evolution is a fundamental approach to constraining the tectonic evolution and climate change influence on an area.

A type example for understanding the dynamic response of drainage network evolution to mountain uplift or climate change lies in southeast Tibet where five major rivers (the Yarlung-Brahmaputra, Irrawaddy, Salween, Mekong, and Yangtze) flow (e.g., Clark et al., 2004; Clift et al., 2006a, b; Nie et al., 2018, Fig. 1). These rivers have very unusual geometries. The Yarlung–Tsangpo River originates in the western Lhasa terrane and flows eastwards along the Yarlung–Tsangpo suture along which India collided with Asia. The river turns sharply to the south at the Eastern Himalayan Syntaxis and changes direction again to flow southwestward after its confluence with the Brahmaputra River. All three rivers of the Salween, Mekong, and Yangtze originate from the eastern part of central Tibet and flow eastward. After approaching the Eastern Himalayan Syntaxis, they flow in parallel to the south for at least 200 km (known as "The Three Parallel Rivers", Fig. 1b), with their drainage basins in considerably closer proximity than would be expected from rivers of their size. The most striking geometry is that of the Yangtze River, which exhibits a sharp turn at Shigu, i.e., the First Bend of the Yangtze (Fig. 1), where the flow direction changes from southeastward to northeastward. These unusual geometries, together with the long wide valley just south of the First Bend of the Yangtze (considered as an abandoned river course (e.g., Lee, 1934; Barbour, 1936)) and the southward flowing Red River (Fig. 1b), make river capture of a paleo-upper Red River (including the upper Yangtze (also called Jinsha River), and possibly the upper Salween and upper Mekong) by the paleo-lower Yangtze, a plausible and intuitive explanation to explain the current drainage pattern (e.g., Brookfield, 1998; Clark et al., 2004).

This drainage network, and its development, receives particular attention with respect to its link with understanding mechanisms of Tibetan evolution and the potential use of drainage changes to constrain the timing of plateau uplift (Hallet and Molnar, 2001; Clark et al., 2004; Yang et al., 2015; Cao et al., 2018; Yuan et al., 2021; Zhao et al., 2021). This is of particular value given the complexities and uncertainties in timing of southeastern plateau uplift as determined from low temperature thermochronology, regional tectonics, and paleoaltimetry studies, with proposed uplift time ranging from Late Cretaceous to Late Miocene (e.g., Clark et al., 2005; Hoke et al., 2014; Zhang et al., 2016; Liu-Zeng et al., 2018; Nie et al., 2018; Tian et al., 2018; 2022; Su et al., 2019; Cao et al., 2020; Li et al., 2020a). Hallet and Molnar (2001) proposed that the large river drainages in the region are antecedent, and their unusual geometries are the result of tectonic deformation by horizontal shear and crustal shortening. By contrast, Clark et al. (2004) proposed that the present drainage configuration is the result of various river captures and drainage reversals away from a previous continental-scale drainage formed at low elevation (Fig. 2); they proposed that the timings of these river captures constrain the timing of eastern Tibetan uplift due to lower crustal flow. However, Yang et al. (2015) suggested that the regional river network was disrupted by tectonic deformation, when the region was already at altitude. More recently, Fox et al., (2020) demonstrated that the assumption of a low-relief surface that has been uplifted and dissected is problematic, and highlighted the need to improve understanding of spatial variations in erodibility including drivers linked to climate change and drainage capture events.

Provenance studies, such as those using the techniques of U–Pb dating of detrital zircon, $^{40}Ar/^{39}Ar$ dating of detrital mica, Sr–Nd bulk rock characterization, and K-feldspar Pb characterization, have been applied to rocks considered to be paleo-river sediments in southeast Tibet, to detect possible provenance changes due to river capture and thereby test the river capture models (e.g. Clift et al., 2004; 2006a, b; 2008; 2020; Hoang et al., 2009; Kong et al., 2009; 2012; Yan et al., 2012; Zhang et al., 2014; 2016; 2017; 2021a; Cao et al., 2015; 2018; Wissink et al., 2016; Chen et al., 2017; Deng et al., 2018; 2020; Zhang et al., 2019a and references therein; Zhang et al., 2019b; Yang et al., 2020; Sun et al., 2020; 2021; Feng et al 2021, He et al., 2021, Zhao et al., 2021; Zhang et al., 2022; Cao et al., 2023; Zhang et al 2023).

Although numerous provenance data have been reported, especially from the most widely employed detrital zircon U–Pb approach, no consensus has been reached. Interpretations can be summarized into two schools of thought. The first school of thought, based on the similar detrital zircon U–Pb spectra between the potential sources of southeastern Tibet and the Cenozoic basins in southeast Tibet, argues that the provenance studies support a connection between the modern upper and middle Yangtze, the upper Mekong, upper Salween, and the modern Red River, i.e. the Greater paleo-Red River, which was captured later by the paleo-lower Yangtze (e.g., Clift et al., 2004; 2020; Hoang et al., 2009; Kong et al., 2012; Yan et al., 2012; Chen et al., 2017), although the capture time is debatably sometime between the Late Cretaceous and Pleistocene. Since the term "paleo-Red River" has been used both to refer to the drainage area of the modern Red River (Fig. 2), and to the hypothetical large dendritic river as proposed by Clark et al. (2004), which includes the upper/middle Yangtze, Yarlung, upper Salween, upper Mekong, Yalong, Dadu and Red rivers, to avoid confusion, we clarify that in this paper we refer to the latter as the "Greater paleo-Red River" (the green dashed area in Fig. 2). The second school of thought, however, argues that the various basin sediments in southeast Tibet can be best explained as locally derived, and therefore do not support a connection between the upper Yangtze, upper Mekong, upper Salween and Red River in the past (Wei et al., 2016; Wissink et al., 2016).

Central to all these provenance studies is the assumption that detrital zircon U–Pb spectra are characteristically different between the various source regions along which the Yangtze and Red River flow, allowing for tracking of detritus from source to sink. Therefore, in this study, we firstly critically appraise this assumption with the most comprehensive zircon U–Pb data compilation of potential source terranes to date (section 2). Secondly, we compile all the published detrital zircon U–Pb data from both the Gonjo (section 3) and Jianchuan (section 4) basins (including our new data) which are proposed to be sediments deposited by a Greater paleo-Red River as explained in more detail below. We assess the evidence for a possible provenance change, and compare these data with the potential source signatures from the various terranes in southeast Tibet. We focused on the Jianchuan Basin as it is located just to the south of the First Bend of the Yangtze River (Fig. 2), and would have received a provenance signal from southeast Tibet if a Greater paleo-Red River once flowed from eastern Tibet through the Jianchuan Basin into the South China Sea, as proposed by a number of previous workers (Yan et al., 2012; Gourbet et al 2017; Clift et al., 2020; Feng et al 2021; He et al 2021; Zheng et al., 2021). We collected data from the Gonjo Basin because it is located in eastern Tibet (Fig. 2), and the massive red beds in the basin are debatably regarded as the fluvial remnants of the paleo-upper Yangtze (Zheng, 2015), which would suggest that the paleo-upper Yangtze was already developed during the deposition of the Gonjo Basin.

Furthermore, given the challenges of using detrital zircon U–Pb data to determining the evolution of the Yangtze and Red rivers as shown in this study, we also carried out a pilot study applying Sr–Nd whole rock and detrital mica $^{40}Ar/^{39}Ar$ analyses to rocks of the Gonjo and Jianchuan Basins, to test whether they might provide good approaches for source discrimination, and hence paleo-drainage reconstruction. Finally, based on all the compiled provenance datasets, we comment on the implications for paleodrainage network evolution in southeast Tibet and future detrital zircon U–Pb studies.

2. Are the different terranes of southeastern Tibet distinguishable in terms of zircon U–Pb spectra?

East and southeast Tibet consist of a series of mosaic blocks that were amalgamated during the opening and closure of the intervening Tethyan oceans. These blocks include the Songpan-Ganzi, Yidun Arc, east and west Qiangtang, Indochina, Sibumasu, and Lhasa terranes (Fig. 1a). Based on paleomagnetic and geological constraints, the north Qiangtang-Indochina collided with North and South China blocks by closing the north branch of the Paleo-Tethys Ocean during the Middle-Late Triassic (e.g., Pullen et al., 2008; Ding et al., 2013; Song et al., 2015; Yan et al., 2019; Guan et al., 2021; Huang et al., 2018; Wu et al., 2020), forming the Songpan-Ganzi flysch as a remnant oceanic basin (Nie et al., 1994; Zhou and Graham, 1996). In the Late Triassic, the south Qiangtang-Sibumasu collided with the north Qiangtang-Indochina due to closure of the southern branch of the Paleo-Tethys Ocean (e.g., Zhao et al., 2015). These events are referred to as the Indosinian Orogeny (e.g., Carter et al., 1999). The Lhasa terrane collided with South Qiangtang during the Late Jurassic-Early Cretaceous (Ma et al., 2018; Li et al., 2019). These above-mentioned collisions, together with the final collision between India and Asia in the early Cenozoic, created the Tibetan Plateau.

To robustly test the drainage capture and evolution model by using detrital zircon U–Pb geochronology, the potential source signatures from the different terranes of southeastern Tibet through which the Yangtze and Red rivers flow, must be clearly distinguishable. Since the modern upper Yangtze drains the east Qiangtang and Songpan-Ganzi terranes, while the Red River headwaters drain over the Indochina terrane and South China Block, it has been argued that if one observes zircon signatures from the Songpan-Ganzi, or east Qiangtang terranes in the Cenozoic rocks of Greater paleo-Red River drainage basins, then a through-flowing river existed from eastern Tibet, connecting the Red River, to the South China Sea.

In previous studies, the characteristic source signatures from these terranes were generally composed from a compilation of zircon U–Pb ages from igneous rocks (e.g., Clift et al., 2008; He et al., 2014). However, we consider that this may ignore the contribution of zircons from sedimentary rocks in these terranes, to the overall terrane signature. Such a contribution is potentially significant as most of the area in these terranes is covered by sedimentary rocks. Therefore, a more representative signature for a terrane may be gained by compiling information from older sedimentary rocks in that terrane. Given that the different terranes in the southeast Tibet were amalgamated after the Middle-Late Triassic (e.g., Pullen et al., 2008; Ding et al., 2013; Song et al., 2015; Faure et al., 2018; Guan et al., 2021), we compiled all available detrital U–Pb zircon grains (n=29545) from sedimentary basin rocks dated from the Middle-Late Triassic in the east Qiangtang terrane, Yidun Arc terrane, Songpan-Ganzi terrane, Indochina terrane, and South China Block (Sichuan Basin and Chuandian sub-terrane) (see supplementary Fig. S1 for data locations and supplementary Table S1 for details). These are all the basins available to characterize the terranes over which the paleo-upper Yangtze and paleo-Red River flowed. Since we compile the sedimentary bedrocks around the Cenozoic basins, this approach can detect if the Cenozoic basin rocks in the Greater paleo-Red River drainage basins may have been locally sourced, as Wissink et al. (2016) suggested.

From the visual comparison of Kernel density estimation (KDE, Fig. 3) using an adaptive bandwidth (same as the other KDE figures) and (nonmetric) multidimensional scaling (MDS, Vermeesch, 2013) plots with bootstrapped confidence regions of the terranes (Supplementary Fig. S2), we note that in most cases, from Late Triassic times onwards, sedimentary rocks from different terranes in southeast Tibet show similar zircon age populations. The dominant five age groups of 200-300 Ma, 400-500 Ma, 700-1100 Ma, 1700-1900 Ma, and 2400-2600 Ma are common peaks in East Asia, associated with the Indosinian, Caledonian, Jinning, Lvliang, and Wutai orogenies, respectively (Wu et al., 2019).

Late Triassic and younger sedimentary rocks cover a significant spatial extent of the various terranes in southeast Tibet, and therefore contribute significant detritus to the Cenozoic sediments. Thus our compilation, which shows that rocks younger than the Late Triassic from the different terranes in southeast Tibet have similar zircon age populations by sedimentary recycling, makes it difficult to obtain a characteristic source signature for these terranes. We illustrate the implications of this proposal in more detail below, by adding new data and a comprehensive review from critical regions of the Gonjo and Jianchuan basins along the length of the drainage route.

The similarity of zircon U–Pb signatures in Late Triassic and younger sedimentary rocks has implications for previous provenance studies. Many previous studies have found that the Cenozoic sedimentary rocks from a series of basins, e.g., Simao, Jianchuan, and Northern Vietnam basins, have similar zircon ages to the Late Triassic rocks in Songpan-Ganzi, or eastern Qiangtang terranes. This has been used as evidence to support the existence of a paleo-upper Yangtze that originated from eastern Tibet and connected to the paleo-Red River in the Early Cenozoic (e.g., Kong et al., 2012; Yan et al., 2012; Chen et al., 2017; Clift et al., 2020; Zheng et al., 2021). However, we suggest that the zircon signature in these basins could also be locally derived by recycling of surrounding older (e.g., Late Triassic-Cretaceous) sedimentary sequences, a proposition recently also proposed by Zhang et al (2023).

We note that Clift et al. (2020) observed that many sedimentary rocks in Cenozoic basins of southeastern Tibet and sediments in rivers of SE Asia contain significant Cenozoic detrital zircon U–Pb aged grains. They argued that these Cenozoic zircon grains can only be sourced from the Qamdo Block (the east Qiangtang terrane in this study) in east Tibet, without recycling, and therefore can be used as a characteristic source signature for a through-flowing river from eastern Tibet. Guo et al. (2021) also used the appearance of Cenozoic detrital zircon U–Pb ages in Miocene sediments of the Jianghan Basin (see Fig. 2 for location) as evidence for the formation of the modern Yangtze. However, as shown in the Jianchuan Basin (see section 4), Cenozoic volcanic rocks are also widespread in Yunnan Province (Chung et al., 2005), and even in the South China Block (e.g., Nanjing area, Fig. 2 for location (Zheng et al., 2013)), suggesting that the Cenozoic zircon grains are also not diagnostic signatures of eastern Tibet.

The sedimentary rocks in the Yidun Arc and South China Sichuan Basin (Figs. 3C and 3E) show a significant change in detrital zircon U–Pb signature between Middle and Late Triassic, shifting from more restricted to more diverse spectra, although this change is not seen in the Songpan-Ganzi terrane. This change may relate to the continued amalgamation of terranes within the Paleo-Tethys Ocean during the Triassic as discussed above, (e.g., Pullen et al., 2008; Ding et al. 2013; Faure et al., 2018; Yan et al., 2019), which may have had a significant influence on sediment routing. Rivers dynamically respond to associated tectonic shortening, concentrating erosion on newly uplifted areas and building new pathways that span the newly accreted terranes, broadening the potential for changes and diversification of provenance. This is evidenced, for example, in the southwestern Sichuan Basin where Yan et al., (2019) noted a major change in sediment routing in response to the Late Triassic closure of the Paleo-Tethys Ocean that drove shortening across the Longmen Shan thrust belt and the eastern Songpan-Ganzi terrane. The zircon U–Pb ages in the Lower–Middle Triassic samples were dominated by Neoproterozoic (~700–900 Ma) zircons sourced mainly from the southwestern South China basement. By contrast, the Upper Triassic samples record multiple peaks, diagnostic of sources within the Qinling, Longmen Shan and Songpan-Ganze terranes (e.g., age peaks at ~270, ~435, ~775, ~1,010, ~1,840 and ~2,480 Ma). However, we acknowledge that the difference may also result from the significant difference in number of grains/samples analyzed between Early-Mid and Late Triassic samples. More pre-Late Triassic analyses from a number of different terranes would be needed to test this hypothesis further.

3. Does the Gonjo Basin sedimentary succession represent deposits of the paleo-upper Yangtze as indicated by detrital zircon U-Pb?

3.1. Age, sedimentology and previous interpretations regarding the Gonjo Basin sedimentary rocks

The > 200 km long Gonjo Basin (30.85°N, 98.3°E, Fig. 4) is located in the eastern part of central Tibet, at the boundary between the Qiangtang and Songpan-Ganzi terranes. It is one of many thrust-bounded basins (e.g., Hoh Xil and Nangqian basins) in the region and is interpreted to have formed as a syn-contractional basin in the footwall of the Yangla fold-thrust system (Studnicki-Gizbert et al., 2008; Tang et al., 2017; Li et al., 2020b; 2020c). The sedimentary strata of the basin are now exposed in an asymmetric syncline, and mainly consist of red-colored mudstones, sandstones, and rare conglomerates, reaching a total thickness of >3000 m (Studnicki-Gizbert et al., 2008; Tang et al., 2017; Li et al., 2020a), and were interpreted as a mixed depositional environment of alluvial fan, fan-delta, floodplain, and lacustrine facies (Studnicki-Gizbert et al., 2008). The sedimentary sequence is divided into the Gonjo Formation and Ranmugou Formation, where the latter is further sub-divided into lower, middle, and upper parts.

The Gonjo Basin was previously assigned an Eocene age based on flora and pollen fossils observed at the top of the succession (Bureau of Geology and Mineral Resources of Xizang Autonomous Region (BGMR Xizang), 1993). However, recent U–Pb and $^{40}Ar/^{39}Ar$ dating on interbedded volcanic rocks (Studnicki-Gizbert et al., 2008; Tang et al., 2017), U–Pb detrital zircon data from sandstones (Zhang et al., 2018; Xiong et al., 2020), together with high resolution magnetostratigraphy, precisely constrains the Gonjo Basin deposition from 69-41.4 Ma (Li et al., 2020b), although Xiao et al. (2021) suggested that the Gonjo Basin ceased deposition in its central part at ~50 Ma.

The current upper Yangtze River flows roughly N-S ~50 km east of the Gonjo Basin, along the Jinsha suture separating the Qiangtang and Yidun Arc terranes. Three Yangtze tributaries flowing south, east, and north to the Gonjo Basin converge in the central part of the basin and then flow to the east to join the Yangtze River (Fig. 4b). Based on detailed sedimentologic, stratigraphic and structural studies of the Gonjo and nearby Nangqian basins, Horton et al. (2002) and Studnicki-Gizbert et al. (2008) concluded that both basins were fed by proximal sources and therefore the large through-going rivers of the Yangtze and Mekong were not developed until deposition ceased in these basins in the Late Eocene. However, Zheng (2015) proposed that the massive red beds in the Gonjo Basin of eastern Tibet are the fluvial remnants of the paleo-upper Yangtze, which would suggest that the paleo-upper Yangtze was already developed since the Eocene. He suggested that this paleo-upper Yangtze could have connected to the paleo-Red River. These ideas are consistent with later detrital zircon studies (He et al., 2021; Zheng et al., 2021) which showed that the zircon U–Pb spectra from the Paleocene-Eocene rocks of the Gonjo and Jianchuan basins (Fig. 2), which are proposed to both be paleo-upper Yangtze deposits (Zheng, 2015), look similar to each other and to the Songpan-Ganzi terrane. Zhang et al. (2019b) albeit also suggested that the Gonjo Basin sediments were mainly sourced from the nearby Songpan-Ganzi terrane, but argued that the Gonjo Basin was an internally drained basin. In this scenario, the upper Yangtze was not established during Late Cretaceous-Eocene deposition of Gonjo Basin sediments.

3.2. Provenance of the Gonjo Basin based on detrital zircon U–Pb data

In order to explore the drainage scenarios based on provenance data derived from detrital zircon U–Pb spectra, as summarized above, we carried out detrital zircon U–Pb analyses from 12 sandstone samples along the magnetostratigraphic section of Li et al. (2020b), with all samples separated by an interval of 2-4 Ma (Fig. 4b). We also analyzed two modern river sediments, one from the modern Yangtze near Gonjo, and one from the eastern side of the Gonjo Basin that drains into the Gonjo Basin (sample Aiyu River, see Fig. 4b for location) Sampling details, U–Pb methods and results are provided in the Supplementary Table S2, S1 and Table S3, respectively. Moreover, we compiled all the published detrital zircon data from the Gonjo Basin.

As shown in Fig. 5, except one sample SY-9 from the upper Ranmugou Formation, all other samples show similar zircon U–Pb age spectra, with minor variations. Most samples show five age groups of 200-300 Ma, 400-500 Ma, 700-1100 Ma, 1700-1900 Ma, and 2400-2600 Ma, some samples also have a Cenozoic age group of 50-60 Ma. Since there are no significant variations of detrital zircon U–Pb spectra over the deposition of the Gonjo Basin, we amalgamated the data into the Late Cretaceous Gonjo Formation, and the Early Cenozoic Ranmugou Formation, and compared them with the potential source signatures.

From visual comparison of the KDE (Fig. 6) and MDS (Supplementary Fig. S3) plots, we show that, apart from a minor 60 Ma age population, the detrital zircon U–Pb age spectra from compiled Gonjo and Ranmugou formations are similar to the Late Triassic Songpan-Ganzi terrane. The Gonjo and Ranmugou formations are also similar to the First Bend of the modern Yangtze. This could suggest that a paleo-upper Yangtze River which originated from the Songpan-Ganzi terrane and flowed through the Gonjo Basin to the First Bend, existed in the Eocene as proposed by Zheng et al. (2021). However, the zircon age spectrum in particular of the Gonjo Formation is also similar to that of the eastern Qiangtang Cretaceous bedrock and to that of the local modern Aiyu River, a small tributary that only cuts through the Triassic and Paleozoic bedrocks to the east of Gonjo Basin (Fig. 5b), demonstrating that a local provenance, e.g., the Qamdo Basin in the southwest (Fig. 5a), could also well explain these Gonjo Basin data. For the 50-60 Ma age population present in the Gonjo Basin, we propose that it could be derived from the surrounding area since magmatic rocks of this age are widespread in the east Qiangtang terrane (e.g., Chung et al., 2005).

In summary, the large compiled detrital zircon dataset from the Gonjo Basin could represent derivation of grains from the Songpan-Ganzi terrane, which could support the concept of a major Eocene River in the region, consistent with the idea that a paleo-upper Yangtze River originated from eastern Tibet at that time (e.g., Zheng et al., 2021 and He et al., 2021). However, the dataset are also consistent with an internal paleodrainage, as proposed by Zhang et al. (2019b). Furthermore, the similarity between zircon age populations of Gonjo Basin sediments and bedrock data from the east Qiangtang terrane and the modern local Aiyu River cannot exclude the possibility of a southwestern or more locally derived provenance for the Gonjo Basin sediments. Indeed, a locally-derived provenance is consistent with the sedimentology and varied paleocurrent directions in the Gonjo Basin (Studnicki-Gizbert et al., 2008, Fig. 4). Therefore, the similarity of the Gonjo detrital zircon U–Pb age spectra to downstream basins cannot be used as conclusive evidence for through-flow of a major drainage, particularly since downstream basin detritus may also be locally-derived (see section 4).

4. Do detrital zircon U-Pb data from the Jianchuan Basin record the drainage capture of the Greater paleo-Red River?

The Jianchuan Basin is located just to the south of the First Bend of the Yangtze River (Fig. 7), and would have received a provenance signal from southeast Tibet if a Greater paleo-Red River once flowed from eastern Tibet through the Jianchuan Basin into the South China Sea. Based on detrital zircon U–Pb analyses, the basin is debatably considered to either have received sediments from a major river of eastern Tibet which could have been the paleo-upper Yangtze River before it was captured by the paleo-lower Yangtze (e.g., Yan et al., 2012; Gourbet et al 2017; Clift et al., 2020; Feng et al 2021; He et al 2021; Zheng et al., 2021) or the basin sediments may be locally derived (Wei et al., 2016; Wissink et al., 2016; Sun et al., 2020a).

4.1. Geological setting of the Jianchuan Basin

The Jianchuan Basin is one of the largest Cenozoic basins on the southeast margin of the Tibetan Plateau. It is located in the southwesternmost part of the South China Block, and bounded by the Qiaohou thrust fault to the west, the Jianchuan strike-slip fault to the east (Fig. 7). The Qiaohou Fault carries Triassic rocks over the Jianchuan Basin and controlled the subsidence and folding of the Basin (Gourbet et al., 2017; Cao et al., 2019). Low-temperature thermochronological data suggest that the Qiaohou Fault was active around 50-39 Ma (Cao et al., 2020). To the west of the Jianchuan Basin lies the Lanping-Simao fold belt (Fig. 7), the northern extension of the Indochina terrane. The Lanping-Simao fold belt is covered mainly by Mesozoic and early Cenozoic red beds (Fig. 7). The Cenozoic Lanping Basin generally has similar stratigraphy to the Jianchuan Basin (Yunnan Bureau of Geology and Mineral Resources (YBGMR), 1990).

4.2. Stratigraphy and sedimentology of the Jianchuan Basin

A major impediment associated with comparison and compilation of previous detrital zircon studies in the Jianchuan Basin is the variations in stratigraphies that different researchers have used. We therefore start by reviewing the stratigraphy and sedimentology of the Jianchuan Basin and note the stratigraphic framework we adopt in this study (Fig. 8).

Based on the geological map of Yunnan Province (YBGMR, 1990), the Jianchuan Basin was previously thought to have accumulated the most continuous sedimentary succession on the southeast margin of Tibet, with a total thickness of more than 6 kilometers. From oldest to youngest, the formations were divided into the Paleocene Yunlong and overlying Guolang formations (sometimes combined as the Mengyejing Formation), the Eocene Baoxiangsi Formation, the Oligocene Jinsichang Formation, the Miocene Shuanghe Formation, and the Pliocene Jianchuan and Sanying Formations (Fig. 8a). However, the ages of these formations were based on limited ostracods, charophyte flora, and plant fossils, and were significantly modified in recent years.

Both the Yunlong and Guolang formations mainly consist of red violet, thin-bedded horizontally-laminated mudrock and marlstone interbedded with red sandstone, interpreted as fluvial floodplain and lacustrine deposits (Wei et al., 2016). Gourbet et al. (2017) merged the Yunlong and Guolang formations together as the Mengyejing Formation, and assigned a Paleocene to early Eocene age to it (Fig. 8c). However, a recent magnetostratigraphic study in the southern part of the Simao Basin (see Fig. 2 for location) suggested that the Mengyejing Formation is Late Cretaceous (~112-63 Ma) (Yan et al., 2021).

The Baoxiangsi Formation consists of massive breccias composed of exclusively angular to subangular, poorly sorted limestone clasts, interbedded with sandstones, conglomerates with basement clasts, and massive red multistorey sandstones with an abundance of planar cross-bedding, with a total thickness of ~800 m (Fig. 8b). The deposits are interpreted as braided fluvial channels with laterally adjacent alluvial fans fed from proximal high relief (Wei et al., 2016; Gourbet et al., 2017). The Jinsichang Formation is mainly comprised of both clast-supported and matrix-supported conglomerates interbedded with coarse sandstones at the bottom, siltstones, mudstones and fine-grained sandstones in the middle, and massive and thick-bedded conglomerates and coarse-grained sandstones at the top (Wei et al., 2016, Fig. 8b). The total thickness of the Jinsichang Formation is considered to be more than 2000 meters, and interpreted as deposited in a braided fluvial environment. Gourbet et al. (2017) merged the Baoxiangsi and Jinsichang formations, considering them to be lateral facies variations. However, as noted by Wei et al. (2016), the varied lithologies of the Baoxiangsi Formation represent diverse facies associations (Figs. 8b and 8c). The breccias are typical debris-flow deposits and the interbedded sandstones represent channel fills. The cross-bedded sandstones of the upper Baoxiangsi Formation were previously considered as evidence of a large river (Clark et al., 2004; Yan et al., 2012; Gourbet et al., 2017; Zheng et al., 2020). However, the surface microscopic characteristics of quartz sand grains and sedimentary structures such as large scale cross-bedding suggest an aeolian origin for the sandstone in the upper part of the Baoxiangsi Formation (Cui et al., 2011). Moreover, Wei et al. (2016) also noted that the Baoxiangsi Formation displays marked lateral facies variations (Fig. 8b), as manifested by distinct facies sequences in different localities. By contrast, the Jinsichang Formation lacks aeolian facies, and the conglomerates and sandstones are best explained as alluvial fan and braided river deposits (Wei et al., 2016). Considering the significantly different lithologies between the Baoxiangsi and Jinsichang Formations, we retain the Baoxiangsi and Jinsichang as separate formations, in agreement with most previous studies (Fig. 8e).

Above the Jinsichang Formation, Gourbet et al. (2017) newly identified a ~100 m carbonate succession which they named as the Jiuziyan Formation. This, and the overlying coal-bearing thinly-laminated mudstones, siltstones and fine sandstones of the Shuanghe Formation are interpreted as palustrine-lacustrine deposits (Gourbet et al., 2017). The Shuanghe Formation was originally assigned as Miocene aged based on the well-known ‘Shuanghe flora’ (YBGMR, 1990). The overlying Jianchuan Formation consists of trachyte, volcanic breccias, and tuffs, interbedded with volcano-sedimentary and pyroclastic rocks, and was assigned as Late Miocene-early Pliocene (YBGMR, 1990). However, Gourbet et al. (2017) dated a number of lava flows and cross-cutting igneous rocks from the Jinsichang and Shuanghe formations, and showed that both formations are Late Eocene rather than Miocene and Pliocene as previously suggested (Fig. 8c). Zheng et al. (2021) proposed that the Jinsichang, Jiuziyan, and Shuanghe formations are coeval lateral facies variations (Fig. 8d), but no any evidence was provided. Therefore, we keep the Jinsichang, Jiuziyan, and Shuanghe formations as separate stratigraphic units following most previous studies (Fig. 8e).

The Sanying Formation is only developed in the southeastern corner of the Jianchuan Basin (Fig. 7). It is mainly comprised of grey and yellow mudstone, interbedded with yellow sandstone and black-greyish lignite (Wang et al., 1998), consistent with deposition in swamp and lacustrine environments. A magnetostratigraphic study suggests a late Miocene-Pleistocene age for the Sanying Formation (Li et al., 2013). Therefore, there are no Oligocene-middle Miocene sediments in the Jianchuan Basin.

4.3. Provenance of the Jianchuan Basin based on detrital zircon U–Pb ages

Previous work utilizing detrital zircon U–Pb data from the sediments of the Jianchuan Basin (Figs. 9-12) have suggested that they are either locally-derived (Wissink et al., 2016) or that they contribute to evidence that a major river once flowed from SE Tibet to the South China Sea (e.g., Clift et al., 2020, He et al., 2021), and was captured by the paleo-lower Yangtze in the late Eocene (e.g., Gourbet et al., 2017, Feng et al., 2021), Oligocene (Yan et al., 2012), or as late as the Quaternary (Kong et al., 2012).

Yan et al. (2012) carried out the first U–Pb detrital zircon study in the Jianchuan Basin. They considered that the zircon U–Pb age spectrum from their sample from the braided fluvial facies of the Baoxiangsi Formation (sample JSJ15, Fig. 9a) looked more similar to the spectrum from the Songpan-Ganzi terrane (see Fig. 3) compared to the sample from the modern Yangtze River First Bend (Fig. 13d, sample from Hoang et al., 2009). They therefore interpreted the Baoxiangsi Formation to be the result of deposition from a major Songpan-Ganzi draining river, rather than the paleo-upper Yangtze draining the Qiangtang terrane. Yan et al. (2012) considered that this major river ceased flowing through the basin after the deposition of the Baoxiangsi Formation, as evidenced by the first record of a more restricted zircon age spectrum, indicative of local drainage, in the Jinsichang Formation above the Baoxiangsi Formation (sample JSJ18, Fig. 10a), although the precise location of this sample in relation to its stratigraphic position is uncertain.

Later workers, e.g., Clift et al. (2020), Zheng et al. (2021), He et al. (2021), and Feng et al. (2021) also concurred with the view that the spectra became more restricted after deposition of the Baoxiangsi Formation. However, they did not make a distinction in terms of whether the Baoxiangsi Formation resembled more the Songpan-Ganzi terrane or a paleo-upper Yangtze River. Instead, they considered that the similarity of the Baoxiangsi Formation to both the Songpan-Ganzi and upper Jinsha signature, as well as to the Gonjo Basin sediments (section 3.2) indicated that the paleo-upper Yangtze used to flow from eastern Tibet through both these basins. In a variant to this view, He et al. (2021) coupled the zircon U–Pb data with geochemistry and heavy mineral data to show that the Jinsichang Formation was more mineralogically mature compared to the Baoxiangsi and Shuanghe Formations. They therefore considered that the Jinsichang Formation represented the paleo-upper Yangtze, whilst the Baoxiangsi and Shuanghe Formations had greater contributions from local proximal sources. Kong et al. (2012), however, carried out a U–Pb detrital zircon study on the Quaternary sediments (Fig. 14b) along the Qiaohou Fault (Fig. 7). They found that the U–Pb age spectra of these Quaternary sediments are also similar to the Songpan-Ganzi terrane (Figs. 14 and 15a), and therefore concluded that a paleo-upper Yangtze drained from southeast Tibet and connected to the Red River through the Jianchuan Basin throughout the Cenozoic until it was captured by the lower Yangtze at 1.7 Ma.

Wissink et al. (2016) conducted a more comprehensive detrital zircon U–Pb study on the Cenozoic sediments from the southeast margin of Tibet, mainly from the Jianchuan and Lanping basins. By comparing the U–Pb ages of all the Cenozoic samples with the potential bedrock sources, they concluded that the provenance of these Cenozoic sediments can be best explained by local derivation, and therefore did not support a connection between the paleo-upper/middle Yangtze and paleo-Red River. However, Gourbet et al. (2017) reconsidered the data from the Jianchuan Basin of Wissink et al. (2016) in the light of their new stratigraphy of the basin. They argued that five of Wissink et al. (2016)'s samples from the upper Baoxiangsi Formation were actually deposited after the time of drainage change from a major through-flowing river to local input as proposed by Yan et al. (2012), while the remaining three samples belonging to the Baoxiangsi Formation have comparable age spectra to those of Yan et al. (2012) (sample JSJ15, Fig. 9a), and therefore were also sourced from the Songpan-Ganzi terrane. They concluded that the massive sandstones of the Baoxiangsi Formation correspond to a major river draining the Songpan-Ganzi which connected a paleo-upper Yangtze with the Red River. They suggested, based on sedimentological evidence, that this major river system was abandoned by the time of deposition of the lacustrine Shuanghe Formation.

From the above, we note that there are three main questions with respect to the provenance of the sediments in the Jianchuan Basin:

Firstly, is the Baoxiangsi Formation detrital zircon spectrum sufficiently similar to the Songpan-Ganzi terrane and dissimilar to the Yangtze First Bend sediments to conclude that the Formation does not represent the paleo-upper Yangtze, as Yan et al. (2012) proposed?

Secondly, do the formations younger than the Baoxiangsi Formation record significant provenance changes due to river capture? Or alternatively, could they still be considered as trunk river sediments, as for example proposed by He et al. (2021), with some previously analyzed samples representing local input that may not represent the dominant facies?

Thirdly, could the Jianchuan basin sediments be locally derived, as Wissink et al. (2016) proposed?

In order to elucidate the three questions posed above, we collected ten samples for U–Pb detrital zircon analysis, four from the Baoxiangsi Formation, two from the Jinsichang

Formation, two from the Shuanghe Formation, and one from each of the Jianchuan and Sanying Formations. We also collected samples from the Late Cretaceous bedrock close to the Jianchuan Basin and modern river sediments at the Yangtze first bend as well as local rivers in the Jianchuan Basin to assess the possibility of locally-derived provenance (Fig. 7, see Supplementary Table S2 for sample details). Furthermore, we compiled all the previously published detrital zircon U–Pb data from the Jianchuan Basin (Supplementary Table S4), as shown in Figs. 9-12. We use the updated stratigraphic framework based on recent new age constraints (see section 4.2 and Fig. 8) for each sample location.

From our compilation, we address the above three questions as follows:

1) Using visual comparison of the KDE plots (Fig. 14), with the acquisition of more data, the spectra from the Songpan-Ganzi and the Yangtze First Bend are insufficiently different from each other to be able to determine whether the Baoxiangsi Formation was derived from one or the other. Specifically, the criteria that Yan et al. (2012) used, namely that the Baoxiangsi Formation matches closely with the Songpan-Ganzi spectrum particularly in terms of a pronounced peak at 1.8-2.0 Ga, and differs from the Yangtze First Bend spectra in terms of the Baoxiangsi Formation lacking Neo- and Meso-Proterozoic grains in the range 1.4-1.8 Ga and 600-1000 Ma, is not upheld. Fig. 14h shows that the Baoxiangsi Formation does have a considerable number of such Neo- and Meso-Proterozoic grains, whilst the more diffuse nature of the 1.6-2.0 Ga peak of the Yangtze First Bend (Fig. 14a) compared to the 1.8-2.0 Ga pronounced peak of the Baoxiangsi Formations and Songpan-Ganzi (Figs. 14h and 14k), is not entirely diagnostic. Similarly, the observation that the Baoxiangsi Formation more closely resembles the Songpan-Ganzi terrane rather than the paleo-upper Yangtze in its lack of Cenozoic young ages (Zhang et al. 2019a) is obviated by new samples from the Baoxiangsi Formation from which young grains are recorded (e.g., Fig. 9j). The discovery of these young ages does not mean, however, that the Baoxiangsi Formation is more likely derived from the

paleo-upper Yangtze, since young volcanic rocks are also prevalent in the Jianchuan Basin (Fig. 7).

Using the MDS plot to determine the degree of similarity between samples (Fig. 15), shows that the Baoxiangsi Formation is similar to both the Songpan-Ganzi terrane and Upper Yangtze First Bend end members, and therefore could be equally well derived from either. Therefore, in summary, the original proposal by Yan et al. (2012), that the Baoxiangsi Formation sediments were deposited by a major river draining the Songpan-Ganzi, which was not the paleo-upper Yangtze, is not upheld with the subsequent inclusion of additional data.

2) A number of previous authors proposed river capture by the time of deposition of the Jinsichang or Shuanghe Formation, based on sedimentological facies criteria (e.g., Gourbet et al. 2017) and the more restricted zircon spectra (e.g., Yan et al. 2012, Feng et al. 2021). However, as already noted by Clift et al. (2020) and Zheng et al. (2021), their four samples from the Jinsichang Formation (JN4 and JN5 from Clift et al. (2020) and JCS-1 and JCS-2 from Zheng et al. (2021), Figs. 10c-f) as well as our two new samples from this formation (JCS5 and JCS6, Figs. 10g, h), show broad zircon age spectra, with very similar age distributions and position on the MDS plot to those of the Baoxiangsi Formation (Fig. 15b). This mix of samples with broad and restricted spectra could be indicative of a major river with additional local input and lateral facies variation, as proposed by He et al. (2021).

The Shuanghe Formation has a significant proportion of Cenozoic zircon U–Pb ages, resulting in it looking considerably different to the other formations (Fig. 14f), and distinct on the MDS (Fig. 15a). However, after excluding grains <60 Ma, the Shuanghe Formation signature is closer to the Baoxiangsi and Jinsichang formations, as shown both in KDE and MDS plots (Figs. 14e and 15b). Thus this formation could still represent a major river, with additional significant input of Cenozoic volcanic zircons derived from local Jianchuan volcanic rocks of this age (see Fig. 7). Furthermore, a number of samples from the Shuanghe Formation overlap with those from the Baoxiangsi and Jinsichang Formations (Fig. 15b), suggesting the possibility that the various samples represent a combination of facies from a through-going river and locally derived deposition.

The only exception to the similar spectra in the formations of the Jianchuan Basin sediments is found in the Jianchuan Formation. In this formation, all the samples have simple age spectra (Fig. 14d) and are dominated by a Cenozoic and 600-900 Ma age populations. The Cenozoic grains may well be derived from the local Jianchuan volcanics like the Shuanghe Formation, whereas the 600-900 Ma age populations are most likely transported by the local eastern river draining from the Yangtze Block into the basin today, which is also dominated by a Neo-Proterozoic age spectrum (Fig. 13h, eastern river to JCB).

Therefore, in summary, the detrital zircon U-Pb data do not rule out that a major river continued to flow through the region, until Jianchuan Formation times. There is not an abrupt change of provenance in the Jianchuan Basin between the Baoxiangsi, Jinsichang, and Shuanghe formations, reflecting the time of river capture when facies changed from a major river to local inputs. Instead, the signature which previously has been interpreted as that of a major river, continues in some samples until the Pliocene or as late as Quaternary (Fig. 14b). Previously documented provenance changes may reflect only that samples were collected from different facies in an intermontane basin, rather than upstream river capture.

3) Both the KDE plots and the MDS plots show that the detrital zircon U–Pb spectra from the Baoxiangsi Formation, Jinsichang Formation, and Shuanghe Formation (excluding grains <60 Ma) look equally similar to the Yangtze First Bend and the local Cretaceous bedrock (Figs. 14 and 15), indicating that a local derivation could well explain the major Jianchuan basin sediments, as proposed by Wissink et al. (2016). The significant young, Cenozoic, grains from the sediments of the Jianchuan Basin may suggest a source from the Qamdo Block, as Clift et al. (2020) suggested. However, these young grains could also be locally derived as

shown by the widespread Cenozoic igneous rocks in the Jianchuan Basin. Therefore, long-distance transport of these young grains from the Qamdo Block is not required. Overall, we have shown that if one is to investigate if local sourcing could produce the observed age spectra, thus negating the need for long distance transport of detritus, comparison with signatures from local older bedrocks and rivers is required.

5. Alternative provenance approaches to investigating river capture: evidence from bulk Sr–Nd isotope and mica $^{40}Ar/^{39}Ar$ analyses?

With the challenges of the use of zircon in providing adequately differentiable source characterization, as described above, we carried out a pilot study applying Sr–Nd whole rock and mica $^{40}Ar/^{39}Ar$ analyses to rocks of the Gonjo and Jianchuan Basins, to test whether they might provide good approaches for source discrimination, and hence paleo-drainage reconstruction, in this region. Our rationale was that, rather than focusing on geological events associated with crystallization (i.e. zircon U–Pb analyses), an approach that focused on timing of cooling of terranes (as determined from mica $^{40}Ar/^{39}Ar$ dating), or distinctive composition of the source rock and the age of crustal material (as determined by Sr–Nd isotopes on bulk rocks), might provide better discrimination between sources.

Although Clift (2016) suggested that both Sr–Nd isotopes and mica $^{40}Ar/^{39}Ar$ ages have many uncertainties as provenance tools in SE Asia, some previous studies have proposed to successfully constrain the capture history of the Greater paleo-Red River and paleo-Yangtze River using these techniques. For example, Hoang et al. (2010) noted a contrast in $^{40}Ar/^{39}Ar$ mica ages between the First Bend of the Yangtze (see Fig. 16 for location, (Triassic-dominated population, Fig. 17v)) and the Red River upper reaches (Cenozoic-dominated population, Figs. 17o-q), and therefore considered that “this method is a good proxy for reconstructing sediment provenance of the Greater paleo-Red River system”. Furthermore, Sun et al. (2020b) compared detrital zircon U–Pb ages and detrital mica $^{40}Ar/^{39}Ar$ ages from the modern Yangtze River drainage basin and demonstrated that different provenance information is provided by these contrasting systems. In particular, they noted that the Dadu tributary to the Min River (see Fig. 16 for location) contains a Cenozoic mica population that may be diagnostic of the paleo-upper Yangtze (Figs. 17s), allowing them to constrain aspects of the capture history by comparison with ancient deposits downstream (Sun et al., 2017; 2021). Additionally, they considered micas from Pliocene sediments in the Jianchuan Basin to be locally derived, thereby constraining the time the Yangtze flowed through the basin as pre-Pliocene (Sun et al., 2020c). Clift et al. (2006a) conducted Sr–Nd analyses on mudstones from the Hanoi Basin at the Red River mouth (see Fig. 16 for location), which shows a rapid shift to less negative εNd values at late Oligocene-early Miocene times (Fig. 18a). They attributed this shift to be the result of the loss of the paleo-middle Yangtze that flowed from the ancient Yangtze craton into the paleo-Red River basin. Although Zhang et al. (2019a) noted that the shift in εNd values may have a much more complex cause, nevertheless, they still considered that the provenance change recorded by Sr–Nd from the Hanoi Basin is 'the strongest line of evidence to date' to support a river reorganization of the Greater paleo-Red River.

5.1. $^{40}Ar/^{39}Ar$ dating of detrital micas as a tool for reconstructing the paleodrainage of the region

Two main strands of research have been undertaken on this topic using detrital mica $^{40}Ar/^{39}Ar$ analyses; one strand has looked at using mica $^{40}Ar/^{39}Ar$ analyses to determine if and when the paleo-upper Yangtze used to drain into the paleo-Red River using the Greater paleo-Red River sediments (Hoang et al., 2010; Sun et al., 2020c), whereas the second strand of research looked at the time when the Yangtze established its current drainage pattern, using paleo-lower Yangtze sediments (Sun et al., 2017; Sun et al., 2021).

5.1.1. Did the paleo-upper Yangtze once flow into the paleo-Red River, as evidenced by mica $^{40}Ar/^{39}Ar$ data?

Given the proposal by Hoang et al. (2010) that mica $^{40}Ar/^{39}Ar$ ages could be a good tool for detecting river capture using the contrasting Triassic and Cenozoic ages from the upper Yangtze and Red River, respectively (see above), we undertook additional analyses at the First Bend of the Yangtze and the Red River head (see Fig. 16 for location) to further test this approach (the methods and results of the $^{40}Ar/^{39}Ar$ mica analyses are provided in the Supplementary materials S2 and Table S5, respectively).

Our new analyses from the Yangtze First Bend concur with Hoang et al. (2010) and Sun et al. (2020c) that show an overwhelming Triassic signal at this location (Figs. 17v). However, our data from the Red River head also show an overwhelming Triassic population (Fig. 17n), compared to the Cenozoic signal at locations further downstream (Figs. 17o-q), the latter presumably more influenced by input from the Cenozoic Ailao Shan-Red River Fault Zone (Clift et al., 2008). The Red River contains both Cenozoic and Triassic populations at its mouth (Fig. 17q). This suggests additional input of a Triassic signal source to the lower stream of the Red River. Given that the Min River tributary to the paleo-middle Yangtze also shows a strong Cenozoic mica peak (Fig. 17s) and is also considered to have flowed into the paleo-Red River in pre-capture times (Clark et al., 2004, Fig. 2), provenance discrimination and thus constraint to capture models based on “Triassic” versus “Cenozoic” diagnostic mica ages is likely more complicated than originally thought.

Sun et al. (2020c) carried out $^{40}Ar/^{39}Ar$ dating and geochemistry of detrital micas in Pliocene sediments from the Jianchuan and Yuanmou basins on the SE margin of Tibet (see Fig. 2 for location), both of which are considered to be regions through which a paleo- upper and -middle Yangtze may have flowed into the paleo-Red River. They showed that muscovite ages from Pliocene Jianchuan Basin sediments overlapped with both the local Yangbi river that drains the Jianchuan Basin (Figs. 17h and 17l) and with the upper Yangtze River, with geochemistry indicating at least some contribution from the upper Yangtze River. By contrast, biotites from the Pliocene Jianchuan Basin sediments had similar ages to a local river draining the basin and a dissimilar signature to the upper Yangtze River. From this they interpreted that the sediments were recycled from the underlying Eocene Baoxiangsi Formation, which previous provenance studies using zircon U–Pb ages proposed to be deposited by the paleo-upper Yangtze River (see section 4). They therefore proposed that the paleo-upper Yangtze had ceased draining into the Jianchuan Basin and hence the Greater paleo-Red River, prior to the Pliocene.

We note that a requirement for local derivation of the biotite grains does not necessarily require a local source also for the muscovite grains, and that the Baoxiangsi Formation may not be derived from the paleo-upper Yangtze (as discussed in section 4). Since no sediments older than the Pliocene in the proposed paleo-upper Yangtze River drainage basins have been subjected to $^{40}Ar/^{39}Ar$ analyses, we collected Paleogene samples from the Gonjo and Jianchuan basins (see Fig. 4 and Fig. 7 for sampling locations). These can be used to test whether $^{40}Ar/^{39}Ar$ muscovite analyses may provide more robust evidence on the evolution of the Greater paleo-Red River, and investigate further the potential for the reworking scenario as suggested by detrital zircon U–Pb (see sections 2-4). For the Gonjo Basin, we collected seven samples for $^{40}Ar/^{39}Ar$ mica dating spanning the Gonjo Paleogene magnetostratigraphic section (Li et al., 2020b). For the Jianchuan Basin, we collected nine samples from the Eocene Baoxiangsi Formation, Late Eocene Jinsichang and Shuanghe formations (but only three samples contained micas suitable for $^{40}Ar/^{39}Ar$ dating), to complement the Pliocene samples published by Sun et al (2020c). The methods and results of the $^{40}Ar/^{39}Ar$ mica analyses are provided in the Supplementary materials S2 and Table S5.

Plotting our new and compiled data from the Jianchuan and Gonjo basins as KDEs (Fig. 17a-k) and MDS plot (Fig. 19), we show that, in both basins, there is little change up section at least since the time of deposition of our oldest sample, with a Triassic age peak dominating throughout, although the Eocene Baoxiangsi Formation has too few data points to allow a robust interpretation. Furthermore, we note that the MDS plot suggests a greater similarity between the Jianchuan Basin sedimentary rocks and the local Yangbi River compared to the Yangtze First Bend, although the number of analyzed mica data is low for the Yangbi River. Therefore, based on the limited available data, we tentatively concur and extend the interpretation of Sun et al. (2020c) that a local provenance is likely for the Jianchuan Basin, at least since the time of deposition of the Jinsichang Formation. However, we stress that more samples are required from the Jianchuan Basin to valid this interpretation in future studies.

Additionally, our new data from the Paleogene Gonjo Basin (Figs. 17a-g) are similar to the data from the Jianchuan Basin (Figs. 17h-k). This might support the proposal that sediments from both these basins have similar provenance, indicating a through-flowing river, as suggested by previous workers using zircon data (e.g., Clift et al., 2020). However, unfortunately, our analyses from the Baoxiangsi Formation are too few for valid comparison, and furthermore, the sediments from the two basins are not exactly co-eval. We do however note that the Gonjo Basin samples overlap in MDS space with the Yangtze River First Bend, and therefore the Gonjo Basin as the headwaters of the paleo-upper Yangtze is viable. Nevertheless, until more samples from local rivers have been analyzed, a local provenance remains equally possible.

5.1.2 When was the Yangtze River formed in its current configuration, as evidenced by mica $^{40}Ar/^{39}Ar$ data?

Sun et al. (2017) conducted a detrital muscovite $^{40}Ar/^{39}Ar$ study on the late Pliocene-Quaternary sediments from the Jianghan Basin (see Fig. 2 for location) through which the modern middle Yangtze flows. They found that the late Pliocene sediments were locally derived whereas the middle Pleistocene sediments contain a unique Cenozoic age population that could only be sourced from eastern Tibet. They therefore concluded that the paleo-lower Yangtze cut through the Three Gorges (see Fig. 2 for location) and reversed the flow direction of the paleo-middle Yangtze between the late Pliocene and middle Pleistocene. They further constrained the lower age limit on the formation of the modern Yangtze by detrital muscovite and K-feldspar dating on the ~Miocene (Zheng et al., 2013) 'Yangtze Gravel' of the lower Yangtze at Nanjing (Sun et al., 2021). Since no Cenozoic aged grains from eastern Tibet were identified in the gravel, they therefore concluded that the current Yangtze was established after the Miocene.

In our data compilation (Fig. 17), it can be seen that the $^{40}Ar/^{39}Ar$ ages along the Yangtze River systematically change from the upper to the lower reaches (see Fig. 16 for sampling locations). They are dominated by Triassic ages at the First Bend of the Yangtze (Fig. 17v), and there is a significant increase of Neoproterozoic ages after the confluence of the Yalong River to the Yangtze (Figs. 17w, x); this is consistent with the dominance of Neoproterozoic mica ages in the Yalong River (Fig. 17r). The $^{40}Ar/^{39}Ar$ ages in the middle and lower reaches of the Yangtze are mainly younger than 120 Ma (Figs. 17y, z, I, II). These characteristic Cretaceous to Cenozoic ages are predominantly recorded in the Min River tributary to the Yangtze (Fig. 17s), and derived from the Longmen Shan belt (through which the Min River flows (Fig 1)) which has common micas of this age (e.g., Kirby et al., 2002; Wallis et al., 2003). Sun et al. (2017; 2021) considered that the Cenozoic $^{40}Ar/^{39}Ar$ ages provide a characteristic signal for the upper Yangtze from eastern Tibet, which can be used to constrain the formation of the modern Yangtze River. However, the $^{40}Ar/^{39}Ar$ ages from the First Bend of the Yangtze (our new data, Hoang et al. (2010), and Sun et al. (2020c), Fig. 17v) and Yalong River (Fig. 17r) show a paucity of these Cenozoic grains. Therefore, since these Cenozoic micas are only found in the Min River, but not in the trunk stream of the upper Yangtze or the Yalong Rivers from eastern Tibet, the appearance of these grains in the lower Yangtze therefore constrains only when the Min River joined the Yangtze system. The capture of the paleo-middle Yangtze (cut through of the Three Georges) and paleo-upper Yangtze and thus what might be considered the "birth of the Yangtze" remains unknown.

5.2. Sr–Nd bulk isotopic data as a technique to determine the paleodrainage of the region

Few studies utilizing bulk rock Sr–Nd to investigate paleodrainage in the region have been undertaken so far (Clift et al., 2004b; 2006; 2008; Liu et al., 2007; He et al., 2021), and no unambiguous agreement has been reached. To further explore the significance of these previous studies, we compiled all published data (see Fig. 16 for sampling locations), and additionally analyzed bulk mudstones from the Cenozoic Gonjo (18 samples, Fig. 4) and Jianchuan (14 samples, Fig. 7) basins and river muds from the modern Red and Yangtze Rivers. Methods are given in Supplementary S3 and results in Table S6 and displayed in Fig. 18.

Clift et al. (2004) noted that εNd values for the Eocene Red River delta in the Gulf of Tonkin (solid green triangles in Fig. 18a) were less negative compared to those of the modern middle upper reaches of the Red River (purple stars), thus requiring that the Eocene material included younger crustal material compared to modern sediment. They proposed two possible interpretations: either the Eocene paleo-Red River included input from the paleo-upper Yangtze, which has modern day values closer to those recorded for the Eocene Gulf of Tonkin (green open triangles in Fig. 18a), or there was additional local contribution from the South China Block to the downstream paleo-Red River record. By contrast, the onshore Hanoi Basin archive of the paleo-Red River shows a major change of εNd values from as low as –17 in the

Eocene, to approximately modern-day values of –11 by the Miocene (Clift et al., 2006a, blue stars in Fig. 18a). Clift et al. (2006a) interpreted this change to reflect drainage loss of the Greater paleo-Red River by separation from the paleo- upper and -middle Yangtze, which flows over the very negative Yangtze Craton. We suggest that the Gulf of Tonkin data is better explained by additional contribution of material with a less negative εNd value to the Red River downstream Hanoi, rather than river capture because 1) the trend to more positive values downstream in the modern Red River (Fig. 18b) supports this hypothesis, and 2) the difference in εNd values between the co-eval Red River repositories of the onshore Hanoi Basin and off-shore Gulf of Tonkin indicates that an additional source must be supplying the offshore.

The trend to more positive εNd values between Eocene to Miocene Hanoi Basin sediments, interpreted as a loss of cratonic input due to capture of the paleo-middle Yangtze away from the Red River (Clift et al., 2006a), seems to provide a more robust argument for river capture. However, as noted by Clift et al. (2008), εNd values show strong variations along the trunk of the Red River, and more significant isotopic variability exists in the smaller tributaries, with some extreme values ranging from an εNd value of –27 to as high as –6 (Fig. 18b). Therefore, we cannot exclude the possibility that the change of εNd values in the Hanoi Basin sediments resulted from changes in Red River tributary input.

He et al. (2021) provided Sr–Nd data from Cenozoic sedimentary rocks from the Jianchuan Basin (see Fig. 7 for sampling locations), previously interpreted to be either locally-derived or the products of a paleo-upper Yangtze draining into the Red River (see section 4). He et al. (2021) complemented their heavy mineral, bulk geochemical, and detrital zircon data from the Jianchuan Basin with Sr–Nd data. They noted a small excursion to more negative εNd values in the Jinsichang Formation compared to the Baoxiangsi and Shuanghe Formations stratigraphically above and below (pink squares in Fig. 18a). They considered that this supported their previous interpretation, as constrained by detrital zircon U–Pb data (see section

4), that a major through-going river of the Greater paleo-Red River developed during the deposition of the Jinsichang Formation. By contrast, our data from the Jinsichang and Shuanghe formations (black solid dots in Fig. 18a) show more variability, and indeed some excursion in the opposite direction to that noted by He et al. (2021). We note that the scatter of data within each formation of the Jianchuan Basin (Fig. 20-biplot) could be consistent with a mix of local derivation and throughput of a major river as previously proposed (section 4.3), although the local Jianchuan river signatures are dissimilar to the basin's Cenozoic sedimentary rocks, except for the Shuanghe Formation, which can be explained by the high prevalence of contemporaneous volcanic material in this Formation.

He et al. (2021) also compared their detrital zircon data from the Jianchuan Basin with those from the Gonjo Basin, using the degree of similarity to interpret a through-going river between these basins. Comparison of Sr–Nd data for approximately co-eval ages (the Baoxiangsi Formation in the Jianchuan Basin (pink triangles in Fig. 20) and Eocene Gonjo (open pink stars in Fig. 20)) between these two basins shows that they plot in broadly different Sr–Nd space albeit with some overlap. This could suggest that, in contrast to the mica (section 5.1) and zircon data (sections 3 and 4), the two basins have dissimilar provenance, not suggestive of a through-going river. Nevertheless, the partial overlap could represent the proposed through-going river, with the non-overlapping samples representing the locally-derived facies. We also note that in the Gonjo Basin, the Cenozoic sedimentary rocks are more similar to the modern local Gonjo River, compared to the upper Yangtze modern River in the Gonjo region, indicating that a paleo-upper Yangtze is not required to explain the Gonjo Basin data.

6. Discussion

6.1. Implications for the evolution of the paleo-Yangtze and Paleo-Red River

Recently, a number of review papers have tried to reconstruct the evolution of Yangtze and Red River in the Cenozoic (Wissink et al., 2016; Zhang et al., 2019a; Clift et al., 2020; Guo et al., 2021; Zhao et al., 2021; Zhang et al., 2021; 2022; Cao et al., 2023; Wang et al., 2023). These review papers all compiled databases, either detrital zircon U–Pb ages, Sr-Nd isotopes, mica $^{40}Ar/^{39}Ar$ ages or Pb isotopes of K-feldspar characterization. Yet a consensus of opinion is yet to be reached. As noted in section 1, most studies that suggest a through-flowing river from east Tibet to the South China Sea are based on the detection of similar detrital zircon U–Pb ages in different basins in southeast Tibet, all considered to be Greater paleo-Red River deposits. Our integrated provenance review of detrital zircon U–Pb data show that the signatures of source areas of the east Qiangtang terrane, Songpan-Ganzi terrane, and Yidun Arc are indistinguishable after the Late Triassic due to zircon recycling and mixing. Therefore, the similar detrital zircon U–Pb spectra from many Cretaceous-Cenozoic basins in southeast Tibet as observed by many previous studies could be either the result of transportation by large rivers, or due to recycling from local bedrocks, and thus cannot be used as solid evidence to support the existence of a large through-flowing river in the Early Cenozoic. The integrated mica $^{40}Ar/^{39}Ar$ and Sr–Nd isotope data from the Cenozoic sediments and modern rivers in southeast Tibet have also not proved to be sensitive provenance discriminators thus far, mainly due to limited data or ambiguity of data interpretations. Overall, the current provenance data determined from zircon U-Pb, mica $^{40}Ar/^{39}Ar$, and Sr–Nd are not sufficiently robust to support the Greater paleo-Red River capture model as many researchers suggested.

Detrital K-feldspar Pb isotopic signatures is currently the most promising avenue documented to determine if and when river capture away from the Greater paleo-Red River occurred. The clearest distinction between source signatures in the region lies with the recognition that the western Yangtze craton where the middle Yangtze flows has feldspars with a less radiogenic signature compared to the Red River (Clift et al., 2008, Zhang et al 2014).

Presence of such grains in the paleo-Red River deposits therefore would indicate prior westward flow of the middle Yangtze into the Red River drainage, with the caveat that such grains can also be delivered to the Red River directly from Red River tributaries that drain the Yangtze craton, such as the Song Lo (Clift et al 2008). The absence of these less radiogenic grains from the Eocene sediments in the onshore Hanoi Basin and the Eocene to Pliocene deposits of the offshore Yinggehai and Qiongdongnan basins suggesting that the middle Yangtze had not flowed into the paleo-Red River at least since the late Eocene (Clift et al 2008; Zhang et al., 2017; 2021a). The upper Yangtze k-feldspar signature, however, is less distinctive, with considerable overlap between signature fields of the Red River and upper Salween (Zhang et al., 2017; 2023), making this method is also insensitive to test whether the upper Yangtze was once connected to the Greater paleo-Red River in the Early Cenozoic.

Considering the different conclusions obtained by different/same provenance methods as shown in this study, it is unlikely to obtain an unambiguous conclusion regarding the drainage network evolution in the southeast margin of Tibet at this stage, but we would advocate that, more $^{40}Ar/^{39}Ar$, Sr–Nd, and Pb isotope researches on Cenozoic sediments in the southeast margin of Tibet, or a combination of these methods, could be effective to solve the Greater paleo-Red River capture model in the future.

6.2. Implications for future detrital zircon U–Pb provenance studies in southeast Tibet

We have shown in sections 3 and 4 that sedimentary recycling plays a fundamental role in the source region detrital zircon signatures after the Late Triassic in southeast Tibet, which was not taken into account by most previous research that used detrital zircon U–Pb dating as a provenance tool to reconstruct paleo-drainage evolution in this region. We propose that after the amalgamation of various terranes (Qiangtang, Indochina, Sibumasu, Songpan-Ganzi) in the Middle-Late Triassic, the ongoing convergence resulted in significant orogeny within these terranes, allowing for development of major rivers crossing the terranes and thus mixed provenance. The potential source terranes of the upland proposed Greater Paleo-Red River are therefore not easily differentiable in terms of having distinguishably different detrital zircon U–Pb spectra. Therefore, the use of detrital zircon U–Pb data in provenance studies to determine paleo-drainage evolution in this region remains challenging, and sedimentary recycling should be considered in more depth in future detrital zircon U–Pb studies in southeast Tibet.

Whilst this paper has focused largely on the role of sedimentary recycling in blurring the provenance signal, the potential degree of influence on the detrital zircon spectra of factors such as source region mineral fertility (e.g., Chew et al., 2020), the effect of hydraulic sorting and facies on the age spectrum (e.g., Yang et al., 2012; Malusà et al., 2016; Sun et al., 2020a), the number of grains required to adequately characterize a sample/site (e.g. Vermeesch et al 2004, Ibanez-mejia et al., 2018) and analytical bias during experimental and data analysis (see review in Chew et al. 2020) is also not well considered in previous studies for this region.

These aspects go beyond the scope of this paper to investigate in detail. However, we noted strong variations of detrital zircon U–Pb age spectra between different samples in the same formation in the Jianchuan Basin, and some samples only have a very restricted age spectra (e.g., JSJ18 in Jinsichang Formation, Fig. 10), which was previous interpreted as evidence of river capture (e.g., Yan et al. 2012). However, when multiple samples are analyzed from the same formation, the data suggest that intra-formational variability may simply record facies variation, with some samples continuing to reflect deposition from a through-flowing river (Fig. 14). This interpretation is best illustrated by detrital zircon U–Pb data from the modern sediments at the First Bend of the Yangtze, which also show strong variation between different studies (Figs. 13c-g), albeit no river capture or provenance change. Moreover, initial apparent differences between the Shuanghe versus other Formations in the Jianchuan Basin, previously also interpreted as evidence of river capture (e.g., Feng et al., 2021), become less significant when the locally derived Cenozoic grains are excluded (Figs 11, 14f, 15), which suggests that local input may create the illusion of provenance change while actually the regional input was still stable, and simply diluted.

7. Conclusions

In order to contribute to the long-disputed controversy on the drainage network reorganization in southeast Tibet and its link with Tibet uplift, we compiled the detrital zircon U–Pb ages used as provenance signatures from the different terranes of southeastern Tibet, to which we added our own new data from the critical regions of the Gonjo and Jianchuan Basins. Our large compiled zircon U–Pb dataset show similar zircon U–Pb spectra between these terranes in upper Triassic and younger rocks, which makes it challenging to clearly distinguish between potential source signatures of the various terranes in southeast Tibet. This similarity of spectra makes it difficult to determine whether sedimentary rocks of the various Cenozoic basins of the region were locally-derived or deposited by long-distance through-flowing rivers. This therefore presents a significant challenge in the use of detrital zircon U–Pb analyses as a provenance tool for documenting paleodrainage evolution in southeast Tibet.

Given the challenges of the zircon U–Pb approach in this setting, we sought to further explore the application of detrital mica $^{40}Ar/^{39}Ar$ analyses and Sr–Nd bulk analyses to this research question. We cautiously uphold the view that these techniques might have promise in certain regions. For example, the Sr-Nd signatures of the Jianchuan and Gonjo Basins are slightly different but with partial overlap, and in the region of the Jianchuan Basin, local rivers have a different Sr–Nd and mica $^{40}Ar/^{39}Ar$ signature to the modern upper Yangtze. However, there is some overlap between the Sr–Nd signatures of the modern Yangtze at the First Bend and the Red River at its source, and strong overlap in their mica $^{40}Ar/^{39}Ar$ signatures, which would also limit the use of these techniques in determining if the paleo-upper Yangtze ever flowed into the paleo-Red River. More analyses are needed to determine if this overlap is significant, or is caused by outliers.

In total, our compiled large dataset suggests that the current provenance data are not sufficiently conclusive to support the Greater paleo-Red River capture model as many researchers suggested, when the influence of zircon sedimentary recycling, inter-sample variation, and local input are taken into consideration.

Acknowledgements

We are grateful to the Editor Harrison Gray, Prof. Ryan Leary and the other two anonymous reviewers for their helpful suggestions and comments which have greatly improved our manuscript. The analysis of zircon U–Pb, mica $^{40}Ar/^{39}Ar$, and Sr–Nd isotope was conducted when SL was a Royal Society postdoctoral researcher at Lancaster University. SL and YN acknowledge support from the Royal Society-K. C. Wong Fellowship and the NIGLFSC (award no. IP-1862-1118 to YN). This research is partly supported by the National Natural Science Foundation of China (41888101). We thank Dr. Su Tao and Shen Zhongshan for field assistance, Dr Zhang Peng, Sun Xilin, and Licheng Cao for insightful discussions.

Open Research

All the data of this manuscript is accessible in the supporting information and will be made on available on Zendo at Li et. al., (2023) https://zenodo.org/record/8152189 upon acceptance.

References

Barbour, G. B., 1936. Physiographic history of the Yangtze. The Geogr. J. 87(1): 17-32.

BGMR Xizang, 1993. Regional Geology of Xizang (Tibet) Autonomous Region. Geological Memoirs Series. Geological House, Beijing.
Brookfield, M., 1998. The evolution of the great river systems of southern Asia during the Cenozoic India-Asia collision: rivers draining southwards. Geomorphology 22, 285-312.
Cao, K., Leloup, P.H., Wang, G., Liu, W., Mahéo, G., Shen, T., Xu, Y., Sorrel, P., Zhang, K., 2020. Thrusting, exhumation, and basin fill on the western margin of the South China block during the India-Asia collision. Geol. Soc. Am. Bull. 133, 74-90.
Cao, K., Wang, G., Leloup, P.H., Mahéo, G., Xu, Y., van der Beek, P.A., Replumaz, A., Zhang, K., 2019. Oligocene-Early Miocene Topographic Relief Generation of Southeastern Tibet Triggered by Thrusting. Tectonics 38, 374-391.
Cao, L., Shao, L., Qiao, P., Zhao, Z., van Hinsbergen, D.J.J., 2018. Early Miocene birth of modern Pearl River recorded low-relief, high-elevation surface formation of SE Tibetan Plateau. Earth Planet. Sci. Lett. 496, 120-131.
Cao, L., Shao, L., van Hinsbergen, D.J., Jiang, T., Xu, D. and Cui, Y., 2023. Provenance and evolution of East Asian large rivers recorded in the East and South China Seas: A review. Geol. Soc. Am. Bull. Doi: 10.1130/B36559.1.
Chen, Y., Yan, M., Fang, X., Song, C., Zhang, W., Zan, J., Zhang, Z., Li, B., Yang, Y., Zhang, D., 2017. Detrital zircon U–Pb geochronological and sedimentological study of the Simao Basin, Yunnan: Implications for the Early Cenozoic evolution of the Red River. Earth Planet. Sci. Lett. 476, 22-33.
Chew, D., Sullivan, G., Caracciolo, L., Mark, C., Tyrrell, S., 2020. Sourcing the sand: Accessory mineral fertility, analytical and other biases in detrital U–Pb provenance analysis. Earth-Sci. Rev. 202, 103093.
Chung, S.-L., Chu, M.-F., Zhang, Y., Xie, Y., Lo, C.-H., Lee, T.-Y., Lan, C.-Y., Li, X., Zhang, Q., Wang, Y., 2005. Tibetan tectonic evolution inferred from spatial and temporal variations in post-collisional magmatism. Earth-Sci. Rev. 68, 173-196.
Clark, M., House, M.A., Royden, L.H., Whipple, K.X., Burchfiel, B.C., Zhang, X., Tang, W., 2005. Late Cenozoic uplift of southeastern Tibet. Geology 33, 525-528.
Clark, M., Schoenbohm, L.M., Royden, L.H., Whipple, K.X., Burchfiel, B.C., Zhang, X., Tang, W., Wang, E., Chen, L., 2004. Surface uplift, tectonics, and erosion of eastern Tibet from large-scale drainage patterns. Tectonics 23, TC1006, doi:10.1029/2002TC001402.
Clift, P., Layne, G., Blusztajn, J., 2004. Marine sedimentary evidence for monsoon strengthening, Tibetan uplift and drainage evolution in East Asia. In: Clift, P.D., Kuknt, W., Wang, P.X., Hayes, D. (Eds.), Continent-Ocean Interactions within East Asian Marginal Seas. American Geophysical Union, Geophys. Monogr. 149, 255-282.
Clift, P., Blusztajn, J., Duc, N.A., 2006a. Large-scale drainage capture and surface uplift in eastern Tibet-SW China before 24 Ma inferred from sediments of the Hanoi Basin, Vietnam. Geophys. Res. Lett. 33, L19403, doi:10.1029/2006GL027772.
Clift, P.D., Carter, A., Campbell, I.H., Pringle, M.S., Van Lap, N., Allen, C.M., Hodges, K.V., Tan, M.T., 2006b. Thermochronology of mineral grains in the Red and Mekong Rivers, Vietnam: Provenance and exhumation implications for Southeast Asia. Geochem. Geophy. Geosy. 7, Q10005, doi:10.1029/2006GC001336.
Clift, P.D., Long, H.V., Hinton, R., Ellam, R.M., Hannigan, R., Tan, M.T., Blusztajn, J., Duc, N.A., 2008. Evolving east Asian river systems reconstructed by trace element and Pb and Nd isotope variations in modern and ancient Red River-Song Hong sediments. Geochem. Geophy. Geosy. 9(4), Q04039, doi:10.1029/2007GC001867.
Clift, P.D., 2016. Assessing effective provenance methods for fluvial sediment in the South China Sea. *From*: Clift, P. D., Harff, J., Wu, J. & Yan, Q. (eds) River-Dominated Shelf Sediments of East Asian Seas. Geological Society, London, Special Publications, 429, doi: 10.1144/SP429.3.

Clift, P.D., Carter, A., Wysocka, A., Long, H.V., Zheng, H., Neubeck, N., 2020. A Late Eocene- Oligocene through-flowing river between the Upper Yangtze and South China Sea. Geochem. Geophy. Geosy. 21, e2020GC009046.

Deng, B., Chew, D., Jiang, L., Mark, C., Cogné, N., Wang, Z., Liu, S., 2018. Heavy mineral analysis and detrital U–Pb ages of the intracontinental Paleo-Yangzte basin: Implications for a transcontinental source-to-sink system during Late Cretaceous time. Geol. Soc. Am. Bull. 130(11-12), 2087-2109.

Deng, B., Chew, D., Mark, C., Liu, S., Cogné, N., Jiang, L., O'Sullivan, G., Li, Z., Li, J., 2020. Late Cenozoic drainage reorganization of the paleo-Yangtze river constrained by multi-proxy provenance analysis of the Paleo-lake Xigeda. Geol. Soc. Am. Bull. 133, 199-211.

Ding, L., Yang, D., Cai, F., Pullen, A., Kapp, P., Gehrels, G., Zhang, L., Zhang, Q., Lai, Q., Yue, Y., 2013. Provenance analysis of the Mesozoic Hoh-Xil-Songpan-Ganzi turbidites in northern Tibet: Implications for the tectonic evolution of the eastern Paleo-Tethys Ocean. Tectonics, 32, 34–48.

Fan, D.D., Li, C.X., Yokoyama, K., Zhou, B.C., Li, B.H., Wang, Q., Yang, S.Y., Deng, B., Wu, G.X., 2005. Monazite age spectra in the Late Cenozoic strata of the Changjiang delta and its implication on the Changjiang run-through time. Science in China, Series D Earth Sciences 48, 1718-1727.

Faure, M., Nguyen, V.V., Hoai, L.T.T., Lepvrier, C., 2018. Early Paleozoic or Early-Middle Triassic collision between the South China and Indochina Blocks: The controversy resolved? Structural insights from the Kon Tum massif (Central Vietnam). J. Asian Earth Sci. 166, 162-180.

Feng, Y., Song, C., He, P., Meng, Q., Wang, Q., Wang, X., Chen, W., 2021. Detrital zircon U-Pb geochronology of the Jianchuan Basin, southeastern Tibetan Plateau, and its implications for tectonic and paleodrainage evolution. Terra Nova 33, 560-572.

Fox. M., Carter, A., Dai, J.G., 2020. How continuous are the "relict" landscapes of southeastern Tibet?. Front. Earth Sci. 8: 587597.

Fu, X., Zhu, W., Geng, J., Yang, S., Zhong, K., Huang, X., Zhang, L., Xu, X., 2021. The present-day Yangtze River was established in the late Miocene: Evidence from detrital zircon ages. J. Asian Earth Sci. 205, 104600.

Gourbet, L., Leloup, P.H., Paquette, J.-L., Sorrel, P., Maheo, G., Wang, G., Yadong, X., Cao, K., Antoine, P.-O., Eymard, I., Liu, W., Lu, H., Replumaz, A., Chevalier, M.-L., Kexin, Z., Jing, W., Shen, T., 2017. Reappraisal of the Jianchuan Cenozoic basin stratigraphy and its implications on the SE Tibetan plateau evolution. Tectonophysics 700-701, 162-179.

Gu, J., Chen, J., Sun, Q., Wang, Z., Wei, Z., Chen, Z., 2014. China's Yangtze delta: Geochemical fingerprints reflecting river connection to the sea. Geomorphology 227, 166-173.

Guan, C., Yan, M.D., Zhang, W.L., Zhang, D.W., Fu, Q., Yu, L., Xu, W.L., Zan, J.B., Li, B.S., Zhang, T., Shen, M.M., 2021. Paleomagnetic and Chronologic Data Bearing on the Permian/Triassic Boundary Position of Qamdo in the Eastern Qiangtang Terrane: Implications for the Closure of the Paleo-Tethys. Geophys. Res. Lett. 48, e2020GL092059.

Hallet, B., Molnar, P., 2001. Distorted drainage basins as markers of crustal strain east of the Himalaya. J. Geophys. Res. 106, 13697-13709.

Hanchar, J.M., Watson, E. Bruce., 2003. Zircon Saturation Thermometry. Reviews in Mineralogy and Geochemistry 53, 89-112.

He, M., Zheng, H., Clift, P.D., 2013. Zircon U–Pb geochronology and Hf isotope data from the Yangtze River sands: Implications for major magmatic events and crustal evolution in Central China. Chem. Geol. 360-361, 186-203.

He, M., Zheng, H., Bookhagen, B., Clift, P.D., 2014. Controls on erosion intensity in the Yangtze River basin tracked by U–Pb detrital zircon dating. Earth-Sci Rev 136, 121-140.

He, M., Zheng, H., Clift, P.D., Bian, Z., Yang, Q., Zhang, B., Xia, L., 2021. Paleogene sedimentary records of the paleo-Jinshajiang (Upper Yangtze) in the Jianchuan Basin, Yunnan, SW China. Geochem. Geophy. Geosy. 22, e2020GC009500.

Hoke, G.D., Liu-Zeng, J., Hren, M.T., Wissink, G.K., Garzione, C.N., 2014. Stable isotopes reveal high southeast Tibetan Plateau margin since the Paleogene. Earth Planet. Sci. Lett. 394, 270-278.

Horton, B.K., Yin, A., Spurlin, M.S., Zhou, J.Y., Wang, J.H., 2002. Paleocene-Eocene syncontractional sedimentation in narrow, lacustrine-dominated basins of east-central Tibet. Geol. Soc. Am. Bull. 114, 771-786.

Huang, B., Yan, Y., Piper, J.D.A., Zhang, D., Yi, Z., Yu, S., Zhou, T., 2018. Paleomagnetic constraints on the paleogeography of the East Asian blocks during Late Paleozoic and Early Mesozoic times. Earth-Sci. Rev. 186, 8-36.

Ibañez-Mejia, M., Pullen, A., Pepper, M., Urbani, F., Ghoshal, G., Ibañez-Mejia, J.C., 2018. Use and abuse of detrital zircon U–Pb geochronology—A case from the Río Orinoco delta, eastern Venezuela. Geology 46, 1019–1022.

Jiao, R., Fox, M., Yang, R., 2022. Late Cenozoic erosion pattern of the eastern margin of the Sichuan Basin: Implications for the drainage evolution of the Yangtze River. Geomorphology 398.

Kang, C. G., Li, C. A., Wang, J. T., & Shao, L., 2009. Heavy minerals characteristics of sediments in Jianghan Plain and its indication to the forming of the Three Gorges. Earth Science-J. China University of Geos. 34(3), 419-427.

Kirby, E., Reiners, P.W., Krol, M.A., Whipple, K.X., Hodges, K.V., Farley, K.A., Tang, W.Q., Chen, Z.L., 2002. Late Cenozoic evolution of the eastern margin of the Tibetan Plateau: Inferences from 40Ar/39Ar and (U-Th)/He thermochronology. Tectonics 21, 1-20.

Kong, P., Granger, D., Wu, F., Caffee, M., Wang, Y., Zhao, X., Zheng, Y., 2009. Cosmogenic nuclide burial ages and provenance of the Xigeda paleo-lake: Implications for evolution of the Middle Yangtze River. Earth Planet. Sci. Lett. 278, 131-141.

Kong, P., Zheng, Y., Caffee, M.W., 2012. Provenance and time constraints on the formation of the first bend of the Yangtze River. Geochem. Geophy. Geosy. 13, Q06017.

Lan, Q., Yan, Y., Huang, C.-Y., Santosh, M., Shan, Y.-H., Chen, W., Yu, M., Qian, K., 2016. Topographic architecture and drainage reorganization in Southeast China: Zircon U-Pb chronology and Hf isotope evidence from Taiwan. Gondwana Res. 36, 376-389.

Lee, C. Y., 1934. The development of the upper Yangtze valley. Bull. Geol. Soc. Chin. 13(1), 107-118.

Li, S.H., Su, T., Spicer, R.A., Xu, C.L., Sherlock, S., Halton, A., Hoke, G., Tian, Y.M., Zhang, S.T., Zhou, Z.K., Deng, C.L., Zhu, R.X., 2020a. Oligocene Deformation of the Chuandian Terrane in the SE Margin of the Tibetan Plateau Related to the Extrusion of Indochina. Tectonics 39, e2019TC005974.

Li, S., van Hinsbergen, D.J.J., Najman, Y., Liu-Zeng, J., Deng, C., Zhu, R., 2020b. Does pulsed Tibetan deformation correlate with Indian plate motion changes? Earth Planet. Sci. Lett. 536, 116144.

Li, S., Hinsbergen, D.J.J., Shen, Z., Najman, Y., Deng, C., Zhu, R., 2020c. Anisotropy of magnetic susceptibility (AMS) analysis of the Gonjo Basin as an independent constraint to date Tibetan shortening pulses. Geophys. Res. Lett. 47, e2020GL087531.

Li, S., Deng, C.L., Yao, H.T., Huang, S., Liu, C.Y., He, H.Y., Pan, Y.X., Zhu, R.X., 2013. Magnetostratigraphy of the Dali Basin in Yunnan and implications for late Neogene rotation of the southeast margin of the Tibetan Plateau. J. Geophys. Res. 118, 791-807.

Li, S., Najman, Y., Vermeesch, P., Barfod, D.N., Millar, I., Carter, A. 2023. A critical appraisal of the sensitivity of detrital zircon U–Pb provenance data to constrain drainage network evolution in southeast Tibet [Data set]. Zenodo. https://doi.org/10.5281/zenodo.8152189.

Liu, X., Chen, J., Maher, B.A., Zhao, B., Yue, W., Sun, Q., Chen, Z., 2018. Connection of the proto-Yangtze River to the East China Sea traced by sediment magnetic properties. Geomorphology 303, 162-171.

Liu-Zeng, J., Zhang, J., McPhillips, D., Reiners, P., Wang, W., Pik, R., Zeng, L., Hoke, G., Xie, K., Xiao, P., Zheng, D., Ge, Y., 2018. Multiple episodes of fast exhumation since Cretaceous in southeast Tibet, revealed by low-temperature thermochronology. Earth Planet. Sci. Lett. 490, 62-76.

Malusà, M. G., Resentini, A., & Garzanti, E., 2016. Hydraulic sorting and mineral fertility bias in detrital geochronology. Gondwana Res. 31, 1-19.

McPhillips, D., Hoke, G.D., Liu-Zeng, J., Bierman, P.R., Rood, D.H., Niedermann, S., 2016. Dating the incision of the Yangtze River gorge at the First Bend using three-nuclide burial ages. Geophys. Res. Lett. 43, 101-110.

Najman, Y., 2005. The detrital record of orogenesis: A review of approaches and techniques used in the Himalayan sedimentary basins. Earth-Sci. Rev. 74, 1-72.

Nie, J.S., Ruetenik, G., Gallagher, K., Hoke, G., Garzione, C.N., Wang, W.T., Stockli, D., Hu, X.F., Wang, Z., Wang, Y., Stevens, T., Danisik, M., Liu, S.P., 2018. Rapid incision of the Mekong River in the middle Miocene linked to monsoonal precipitation. Nat. Geosci. 11, 944-949.

Nie, S.Y., Yin, A., Rowley, D.B., Jin, Y.G., 1994. Exhumation of the Dabie-Shan Ultra High-Pressure Rocks and Accumulation of the Songpan-Ganzi Flysch Sequence, Central China. Geology 22, 999-1002.

Pullen, A., Kapp, P., Gehrels, G.E., Vervoort, J.D., Ding, L., 2008. Triassic continental subduction in central Tibet and Mediterranean-style closure of the Paleo-Tethys Ocean. Geology 36, 351-354.

Studnicki-Gizbert, C., Burchfiel, B.C., Li, Z., Chen, Z., 2008. Early Tertiary Gonjo basin, eastern Tibet: Sedimentary and structural record of the early history of India-Asia collision. Geos. 4, 713-735.

Su, T., Spicer, R.A., Li, S.-H., Xu, H., Huang, J., Sherlock, S., Huang, Y.-J., Li, S.-F., Wang, L., Jia, L.-B., Deng, W.-Y.-D., Liu, J., Deng, C.-L., Zhang, S.-T., Valdes, P.J., Zhou, Z.-K., 2019. Uplift, climate and biotic changes at the Eocene–Oligocene transition in south-eastern Tibet. Nat. Sci. Rev. 0, 1-10.

Sun, X., Kuiper, K.F., Tian, Y., Li, C.a., Gemignani, L., Zhang, Z., Wijbrans, J.R., 2020a. Impact of hydraulic sorting and weathering on mica provenance studies: An example from the Yangtze River. Chem. Geol. 532, 119359.

Sun, X., Kuiper, K.F., Tian, Y., Li, C.a., Zhang, Z., Gemignani, L., Guo, R., de Breij, V.H.L., Wijbrans, J.R., 2020b. 40Ar/39Ar mica dating of late Cenozoic sediments in SE Tibet: implications for sediment recycling and drainage evolution. J. Geol. Soc. 177(4), 843-854.

Sun, X., Kuiper, K.F., Tian, Y., Li, C.a., Zhang, Z., Wijbrans, J.R., 2020c. Comparison of Detrital zircon U–Pb and muscovite ^{40}Ar/^{39}Ar ages in the Yangtze sediment: Implications for provenance studies. Minerals 10(7), 643.

Sun, X., Tian, Y., Kuiper, K.F., Li, C.a., Zhang, Z., Wijbrans, J.R., 2021. No Yangtze River prior to the Late Miocene: Evidence from detrital muscovite and K-feldspar ^{40}Ar/^{39}Ar geochronology. Geophys. Res. Lett. 48, e2020GL089903.

Tang, M., Liu-Zeng, J., Hoke, G.D., Xu, Q., Wang, W., Li, Z., Zhang, J., Wang, W., 2017. Paleoelevation reconstruction of the Paleocene-Eocene Gonjo basin, SE-central Tibet. Tectonophysics 712-713, 170-181.

Tian, Y., Kohn, B.P., Qiu, N., Yuan, Y., Hu, S., Gleadow, A.J.W., Zhang, P., 2018. Eocene to Miocene out-of-sequence deformation in the eastern Tibetan Plateau: insights from shortening structures in the Sichuan Basin. J. Geophy. Res. 123, doi: 10.1002/2017JB015049.
Tian, Y., Liu, Y., Li, R., Sun, X., Zhang, Z., Carter, A., Vermeesch, P., 2022. Thermochronological constraints on Eocene deformation regime in the Long-Men Shan: Implications for the eastward growth of the Tibetan Plateau. Global Planet Change 217, 103930.
Hoang, L., Clift, P.D., Mark, D., Zheng, H., Tan, M.T., 2010. Ar–Ar muscovite dating as a constraint on sediment provenance and erosion processes in the Red and Yangtze River systems, SE Asia. Earth Planet. Sci. Lett. 295, 379-389.
Hoang, L., Wu, F.-Y., Clift, P.D., Wysocka, A., Swierczewska, A., 2009. Evaluating the evolution of the Red River system based on in situ U–Pb dating and Hf isotope analysis of zircons. Geochem. Geophy. Geosy. 10, Q11008.
Vermeesch, P., 2004. How many grains are needed for a provenance study? Earth Planet. Sci. Lett. 224, 441-451.
Vermeesch, P., 2013. Multi-sample comparison of detrital age distributions. Chem. Geol. 341, 140-146.
Wang, E., Burchfiel, B.C., Royden, L.H., Chen, L.Z., Chen, J.S., Li, W.X., Chen, Z.L., 1998. Late Cenozoic Xianshuihe-Xiaojiang, Red River, and Dali Fault Systems of Southwestern Sichuan and Central Yunnan, China. Geol. Soc. Am. Special Paper 327, 1-108.
Wallis, S., Tsujimori, T., Aoya, M., Kawakami, T., Terada, K., Suzuki, K., Hyodo, H., 2003. Cenozoic and Mesozoic metamorphism in the Longmenshan orogen: Implications for geodynamic models of eastern Tibet. Geology 31, 745-748.
Wei, H.-H., Wang, E., Wu, G.-L., Meng, K., 2016. No sedimentary records indicating southerly flow of the paleo-Upper Yangtze River from the First Bend in southeastern Tibet. Gondwana Res. 32, 93-104.
Wissink, G.K., Hoke, G.D., Garzione, C.N., Liu-Zeng, J., 2016. Temporal and spatial patterns of sediment routing across the southeast margin of the Tibetan Plateau: Insights from detrital zircon. Tectonics, 35, doi:10.1002/2016TC004252.
Wu, F., Wan, B., Zhao, L., Xiao, W., Zhu, R., 2020. Tethyan geodynamics, Acta Petrol. Sin. 36(6), 1627-1674.
Xiong, Z., Ding, L., Spicer, R.A., Farnsworth, A., Wang, X., Valdes, P.J., Su, T., Zhang, Q., Zhang, L., Cai, F., Wang, H., Li, Z., Song, P., Guo, X., Yue, Y., 2020. The early Eocene rise of the Gonjo Basin, SE Tibet: From low desert to high forest. Earth Planet. Sci. Lett. 543, 116312.
Yan, M., Zhang, D., Fang, X., Zhang, W., Song, C., Liu, C., Zan, J., Shen, M., 2021. New insights on the age of the Mengyejing Formation in the Simao Basin, SE Tethyan domain and its geological implications. Sci. China Earth Sci. 64, 231-252.
Yan, Y., Carter, A., Huang, C.-Y., Chan, L.-S., Hu, X.-Q., Lan, Q., 2012. Constraints on Cenozoic regional drainage evolution of SW China from the provenance of the Jianchuan Basin. Geochem. Geophy. Geosy. 13, Q03001.
Yan, Z., Tian, Y., Li, R., Vermeesch, P., Sun, X., Li, Y., Rittner, M., Carter, A., Shao, C., Huang, H., Ji, X., 2019. Late Triassic tectonic inversion in the upper Yangtze Block: Insights from detrital zircon U-Pb geochronology from south-western Sichuan Basin. Basin Res. 31, 92-113.
Yang, C., Shen, C., Zattin, M., Yu, W., 2021. Formation of the Yangtze Three Gorges: Insights from detrital apatite fission-track dating of sediments from the Jianghan Basin. Terra Nova 00, 1-10.

Yang, R., Willett, S.D., Goren, L., 2015. In situ low-relief landscape formation as a result of river network disruption. Nature 520, 526-529.

Yang, R., Suhail, H.A., Gourbet, L., Willett, S.D., Fellin, M.G., Lin, X., Gong, J., Wei, X., Maden, C., Jiao, R., Chen, H., 2020. Early Pleistocene drainage pattern changes in Eastern Tibet: Constraints from provenance analysis, thermochronometry, and numerical modeling. Earth Planet. Sci. Lett. 531, 115955.

Yang, S., Li, C., Yokoyama, K., 2006. Elemental compositions and monazite age patterns of core sediments in the Changjiang Delta: Implications for sediment provenance and development history of the Changjiang River. Earth Planet. Sci. Lett. 245, 762-776.

Yang, S., Zhang, F., & Wang, Z., 2012. Grain size distribution and age population of detrital zircons from the Changjiang (Yangtze) River system, China. Chemical Geology 296, 26-38.

Yuan, S., Li, C., Zhang, Y., Shao, L., Wang, J., 2012. Trace element characteristics of sediments in Jianghan Basin: Implications for expansion of the upper reaches of the Yangtze River. Geology in China 39, 1042-1048.

Yuan, X.P., Huppert, K.L., Braun, J., Shen, X., Liu-Zeng, J., Guerit, L., Wolf, S.G., Zhang, J.F., Jolivet, M., 2021. Propagating uplift controls on high-elevation, low-relief landscape formation in the southeast Tibetan Plateau. Geology 50 (1): 60–65.

Yue, W., Jin, B., Zhao, B., 2018. Transparent heavy minerals and magnetite geochemical composition of the Yangtze River sediments: Implication for provenance evolution of the Yangtze Delta. Sediment. Geol. 364, 42-52.

Yunnan Bureau of Geology and Mineral Resources (YBGMR), 1990. Regional geology of Yunnan Province. Geological Publishing House, Beijing, 1-726 (In Chinese).

Zhang, H., Oskin, M.E., Liu-Zeng, J., Zhang, P., Reiners, P.W., Xiao, P., 2016. Pulsed exhumation of interior eastern Tibet: Implications for relief generation mechanisms and the origin of high-elevation planation surfaces. Earth Planet. Sci. Lett. 449, 176-185.

Zhang, P., Najman, Y., Mei, L., Millar, I., Sobel, E., Carter, A., Barfod, D., Dhuime, B., Garzanti, E., Govin, G., Vezzoli, G., Hu, X., 2019a. Palaeodrainage evolution of the large rivers of East Asia, and Himalayan-Tibet tectonics. Earth-Sci. Rev. 192, 601-630.

Zhang, Y., Huang, W., Huang, B., van Hinsbergen, D.J.J., Yang, T., Dupont-Nivet, G., Guo, Z., 2018. 53-43 Ma deformation of the Eastern Tibet revealed by three stages of tectonic rotation in the Gongjue basin. J. Geophys. Res. 123, 3320-3338.

Zhang, Y., Huang, W., Zhang, Y., Poujol, M., Guillot, S.R., P. Dupont-Nivet, G. Guo, Z., 2019b. Detrital zircon provenance comparison between the Paleocene-Eocene Nangqian-Xialaxiu and Gongjue basins: New insights for Cenozoic paleogeographic evolution of the eastern Tibetan Plateau. Palaeogeogr Palaeocl 533, 109241.

Zhang, Z., Daly, J.S., Li, C.a., Tyrrell, S., Sun, X., Yan, Y., 2017. Sedimentary provenance constraints on drainage evolution models for SE Tibet: Evidence from detrital K-feldspar. Geophys. Res. Lett. 44, 4064-4073.

Zhang, Z., Daly, J.S., Li, C.a., Tyrrell, S., Sun, X., Badenszki, E., Li, Y., Zhang, D., Tian, Y., Yan, Y., 2021a. Formation of the Three Gorges (Yangtze River) no earlier than 10 Ma. Earth-Sci. Rev. 216, 103601.

Zhang, Z., Daly, J.S., Yan, Y., Lei, C., Badenszki, E., Sun, X., Tian, Y., 2021b. No connection between the Yangtze and Red rivers since the late Eocene. Mar. Pet. Geol. 129, 105115.

Zhang, Z., Daly, J.S., Tian, Y., Wang, Y., Badenszki, E., Sun, X., Liu, Y., 2023. Sedimentary recycling in Jianchuan Basin, SE Tibetan Plateau: A solution to the debate on the formation age of the First Bend (Yangtze River). Geomorphology 108888.

Zhang, Z., Tyrrell, S., Li, C.a., Daly, J.S., Sun, X., Li, Q., 2014. Pb isotope compositions of detrital K-feldspar grains in the upper-middle Yangtze River system: Implications for sediment provenance and drainage evolution. Geochem. Geophy. Geosy. 15, 2765-2779.

Zhao, M., Shao, L., Liang, J., Li, Q., 2015. No Red River capture since the late Oligocene: Geochemical evidence from the Northwestern South China Sea. Deep Sea Research Part II: Topical Studies in Oceanography 122, 185-194.
Zhao, X., Zhang, H., Hetzel, R., Kirby, E., Duvall, A.R., Whipple, K.X., Xiong, J., Li, Y., Pang, J., Wang, Y., Wang, P., Liu, K., Ma, P., Zhang, B., Li, X., Zhang, J., Zhang, P., 2021. Existence of a continental-scale river system in eastern Tibet during the late Cretaceous-early Palaeogene. Nat. Commun. 12, 7231.
Zheng, H., 2015. Birth of the Yangtze River: age and tectonic-geomorphic implications. Natl. Sci. Rev. 2, 438-453.
Zheng, H., Clift, P.D., He, M., Bian, Z., Liu, G., Liu, X., Xia, L., Yang, Q., Jourdan, F., 2021. Formation of the First Bend in the late Eocene gave birth to the modern Yangtze River, China. Geology 49, 35-39.
Zheng, H., Clift, P.D., Wang, P., Tada, R., Jia, J., He, M., Jourdan, F., 2013. Pre-Miocene birth of the Yangtze River. Proc. Natl. Acad. Sci. USA 110, 7556-7561.
Zhou, D., Graham, S. A., 1996. Songpan-Ganzi Triassic flysch complex of the West Qinling Shan as a remnant ocean basin. In: Yin, A., Harrison M. (Eds.), The tectonic evolution of Asia, 281-299.
Zutterkirch, I.C., Kirkland, C.L., Barham, M., Elders, C., 2022. Thin-section detrital zircon geochronology mitigates bias in provenance investigations. J. Geol. Soc. 179, jgs2021-070.

Supplementary information

The supplementary file includes the method for detrital zircon U–Pb (Supplementary S1), mica $^{40}Ar/^{39}Ar$ (Supplementary S2), Sr–Nd bulk rock (Supplementary S3) analyses, and details of supplementary figures (Supplementary Figure S1-S3), the compilation of previous zircon U–Pb datasets (Supplementary Table S1), and the sampling details of this study (Supplementary Table S2), U–Pb results from the Gonjo Basin (Supplementary Table S3), Jianchuan Basin (Supplementary Table S4), $^{40}Ar/^{39}Ar$ results (Supplementary Table S5), and Sr–Nd results (Supplementary Table S6).

Figure Captions

Figure 1. (a) Map illustrating the major geological terranes and the major fluvial drainages in East and SE Asia. (b) Enlarged map (green doted square in Fig. 1a) showing the Three Parallel Rivers (TPR) and the First Bend of Yangtze (FB). Abbreviations: TH: Tethyan Himalaya, LH: Lhasa terrane, E/WQT: East/West Qiangtang terrane, SPGZ: Songpan-Ganzi terrane, YD:

Yidun Arc, WB: West Burma Block, SI: Sibumasu terrane. AKMS: Anyimaqin-Kunlun-Muztagh suture, QL-DB: Qinling-Dabie, JSJS: Jinshajiang suture, LMC-SH: Longmuco-Shuanghu suture, BG-NJ: Bangonghu-Nujiang suture, IYS: Indus-Yarlung suture, CN-ML: Changning-Menglian suture, I-BT-R: Inthanon-Bentong-Raub suture, SM: Songma suture, GZLT: Ganzi-Litang suture. EHS: Eastern Himalayan syntaxis, IBR: Indo-Burman Ranges, FB: the First Bend of Yangtze, SGF: Sagaing Fault, LMST: Longmenshan Thrust Fault, SCB: Sichuan Basin, TG: Three Gorges, JHB: Jianghan Basin, HB: Hanoi Basin, SHYB: Songhong-Yinggehai Basin.

Figure. 2: The Greater paleo-Red River (green dashed area) capture model as proposed by Clark et al. (2004). The orange areas denote main sedimentary basins discussed in this study. Modified after Clark et al. (2004) and Zhang et al. (2019). NQ: Nangqian Basin, GJ: Gonjo Basin, FB: the First Bend of Yangtze, LPB: Lanping Basin, JCB: Jianchuan Basin, CXB: Chuxiong Basin, YMB: Yuanmou Basin, YJB: Yuanjiang Basin, N Vietnam: North Vietnam Basin, SCB: Sichuan Basin, TG: Three Gorges, JHB: Jianghan Basin, NJ: Nanjing.

Figure 3. Kernel Density Estimation (KDE) plots for the compiled U–Pb detrital zircon data from different geological domains on the eastern margin of Tibet. The five grey bars indicate the common zircon populations seen in East Asia, associated with the Indosinian orogeny, Caledonian orogeny, Jinning orogeny, Lvliang orogeny, and Wutai orogeny, respectively (Wu et al., 2019)

Figure 4. (A) Geological map of southeastern Tibet showing the Gonjo and Nangqian basins. B) Enlarged geological map of the Gonjo Basin showing the locations of U–Pb sampling sites of previous work and this study. Arrows with circles denote the paleocurrent directions, data

are from Studnicki-Gizbert et al. (2008) and Tang et al. (2017). The abbreviations are the same as Fig. 1 and Fig. 4.

Figure 5. KDE plots of all detrital zircon U–Pb ages from sedimentary rocks of the Gonjo Basin in stratigraphic order, including published data as referenced. The grey vertical bars indicate the common zircon populations in East Asia as stated in Fig. 4.

Figure 6. Detrital zircon U–Pb data from the Gonjo Basin compared to various source regions. KDE plots of detrital zircon U–Pb ages from the Gonjo Basin (GJ) Gonjo (a) and Ranmugou (b) formations, compared to modern local rivers draining into the Gonjo Basin from the underlying Qiangtang terrane (Aiyu River, c), modern river sediment from the Yangtze River at Gonjo (d), Late Triassic sedimentary rocks from East Asian terranes (e-h), and modern river First Bend of Yangtze (YZ_FB, i).

Figure 7. Geological map of the Jianchuan Basin and surrounding area, modified after BRGMY (1990) and Cao et al. (2021). The sampling locations of detrital zircon U–Pb, $^{40}Ar/^{39}Ar$, and Sr–Nd of previous work and this study are marked by different symbols. Arrows with circles denote the paleocurrent directions, data are from Wei et al. (2016), Wissink et al. (2016), and He et al. (2021).

Figure 8. Diagram showing the different stratigraphic frameworks proposed for the Jianchuan Basin.

Figure 9. KDE plots of the detrital zircon U–Pb ages from individual samples of the Baoxiangsi formation in the Jianchuan Basin from previous work and this study. The published data are

from Yan et al. (2012), Kong et al. (2012), Wissink et al. (2016), Clift et al. (2020), Zheng et al. (2020), He et al. (2021), and Feng et al. (2021). The five vertical bars indicate the common zircon populations in East Asia as stated in Fig. 4. The yellow vertical bar indicates the Cenozoic zircon populations that may be derived from the volcanic rocks in the Jianchuan basin.

Figure 10. KDE plots of the detrital zircon U–Pb ages from individual samples of the Jinsichang Formation in the Jianchuan Basin from previous work and this study. The vertical bars are the same as Fig. 9.

Figure 11. KDE plots of the detrital zircon U–Pb ages from individual samples of the Shuanghe Formation in the Jianchuan Basin from previous work and this study. The vertical bars are the same as Fig. 9.

Figure 12. KDE plots of the detrital zircon U–Pb ages from individual samples of the Jianchuan and Sanying formations in the Jianchuan Basin from previous work and this study. The vertical bars are the same as Fig. 9.

Figure 13. KDE plots of the detrital zircon U–Pb ages from modern Yangtze River samples at Tuotuohe (a, head of the Yangtze, He et al. 2013), at Gonjo (b, this study), and at the First Bend of Yangtze (c-g), as well as local rivers draining in to Jianchuan Basin (h-j). The vertical bars are the same as Fig. 9.

Figure 14. KDE plots of detrital zircon U–Pb ages, combining all samples for each formation in the Jianchuan Basin (b-h) and comparisons with the Yangtze First Bend (YZ_FB, a),

Cretaceous sedimentary bedrocks around the Jianchuan Basin (i), a local river from the eastern side of the Jianchuan Basin (j), and Late Triassic sedimentary bedrocks from Songpan-Ganzi (k), Yidun Arc (l) and Qiangtang (n) terranes. The vertical bars are the same as Fig. 9.

Figure 15. (a) MDS plot using the data of Fig. 14. (b) MDS plot using all the individual samples from the Jianchuan Basin, data from Figs 9-12. The two Baoxiangsi and Jinsichang Formation samples interpreted by Wissink et al. (2016) as transverse fluvial facies are depicted by a cross through the symbols. T2 = Mid Triassic, T3=Late Triassic, J1, 2 and 3 = Early, Middle, and Late Jurassic, K1 and 2 = Early and Late Cretaceous, Pg = Paleogene, Mio = Miocene, Plio=Pliocene, Q=Quaternary.

Figure 16. Map showing the sampling locations for mica $^{40}Ar/^{39}Ar$ and Sr-Nd bulk sample analyses from modern rivers analyzed in previous published research and this study.

Figure 17. $^{40}Ar/^{39}Ar$ ages (as probability density plots) of detrital mica samples from Gonjo Basin (a-g), Jianchuan Basin (h-k), Yangbi river (l), Mekong River mouth (m), Red Rivers (n-q), tributary rivers of the Yangtze (r-u), and the main Yangtze (v-II).

Figure 18. (a) Strontium ($^{87}Sr/^{86}Sr$) and neodymium (εNd) data from the Jianchuan and Gonjo basins (this study and from He et al. (2021)) compared to previous data from the Hanoi Basin (Clift et al., 2006), Gulf of Tonkin (Clift et al., 2004), and various modern rivers (data are from Clift et al., 2004; 2008; Liu et al., 2007). (b) Diagram showing the downstream variation in $^{87}Sr/^{86}Sr$ and εNd values from the Red River trunk and its small tributaries.

Figure 19. MDS plots of the $^{40}Ar/^{39}Ar$ ages in Fig. 16. The dashed circle symbol of JC_Baoxiangsi refers to the low number n of analyses from the Baoxiangsi Formation which makes the data potentially unreliable.

Figure 20. Bi-plot of the strontium ($^{87}Sr/^{86}Sr$) and neodymium (εNd) data in Fig. 18.

Figure 1.

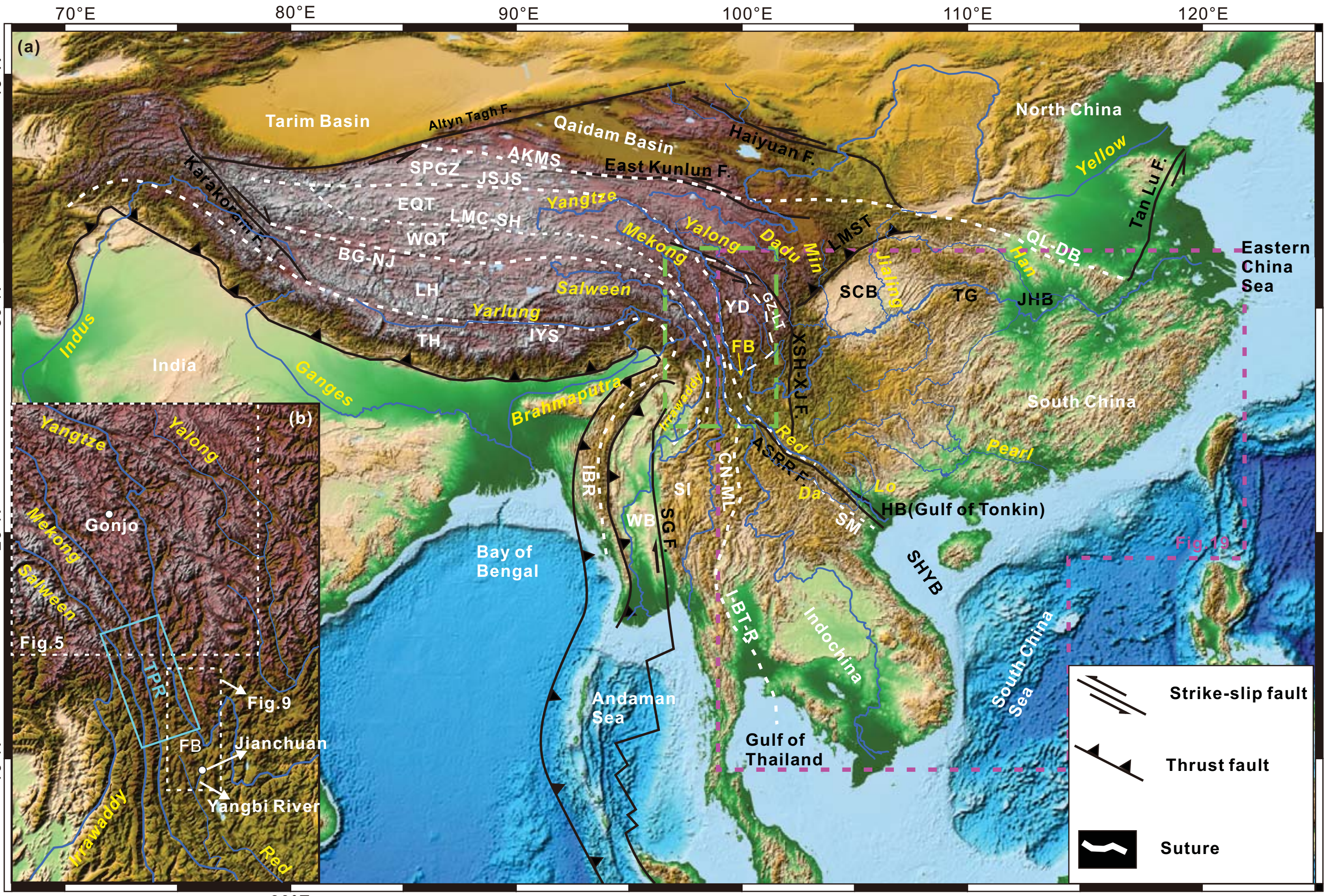

70°E
80°E
90°E
100°E
110°E
120°E
40°N
30°N
20°N
10°N
(a)
Tarim Basin
Altyn Tagh F.
Qaidam Basin
Haiyuan F.
North China
Yellow
Tan Lu F.
AKMS
SPGZ
JSJS
East Kunlun F.
Karakoram F.
EQT
LMC-SH
Yangtze
WQT
BG-NJ
Mekong
Yalong
Dadu
Min
LMST
QL-DB
Han
Eastern China Sea
LH
Salween
YD
GZLT
SCB
Jialing
TG
JHB
Yarlung
TH
IYS
Indus
India
Ganges
FB
XSH-XJF
Brahmaputra
South China
Irrawaddy
Red
Pearl
IBR
CN-ML
ASRR F.
SI
Da
Lo
WB
SG F.
SM
HB(Gulf of Tonkin)
Bay of Bengal
SHYB
Fig.19
IBT-B
Indochina
South China Sea
Andaman Sea
Gulf of Thailand
Strike-slip fault
Thrust fault
Suture
(b)
Yangtze
Yalong
Gonjo
Mekong
Salween
Fig.5
TPR
Fig.9
FB
Jianchuan
Yangbi River
Irrawaddy
Red

Figure 2.

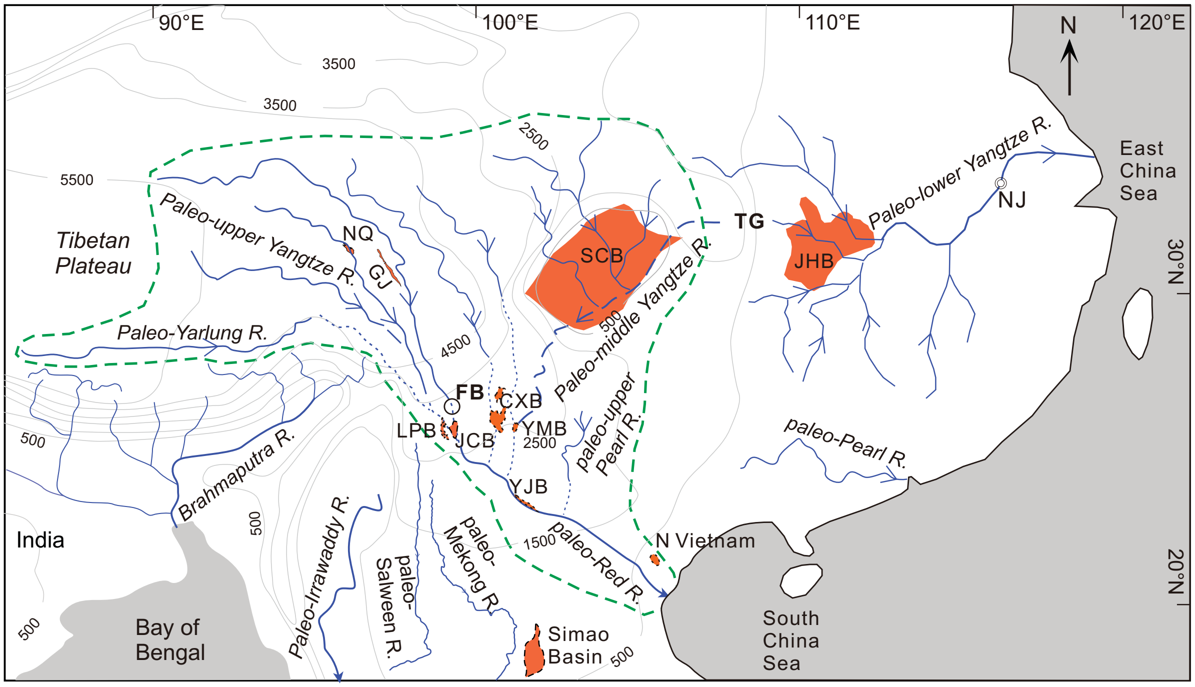
90°E
100°E
110°E
120°E
N
3500
3500
5500
2500
4500
500
2500
1500
500
500
500
500
Tibetan Plateau
Paleo-upper Yangtze R.
NQ
GJ
SCB
TG
JHB
Paleo-lower Yangtze R.
NJ
East China Sea
30°N
Paleo-Yarlung R.
Paleo-middle Yangtze R.
FB
CXB
YMB
LPB
JCB
paleo-upper Pearl R.
paleo-Pearl R.
Brahmaputra R.
India
YJB
paleo-Red R.
N Vietnam
20°N
paleo-Mekong R.
paleo-Salween R.
Paleo-Irrawaddy R.
Bay of Bengal
Simao Basin
South China Sea

Figure 3.

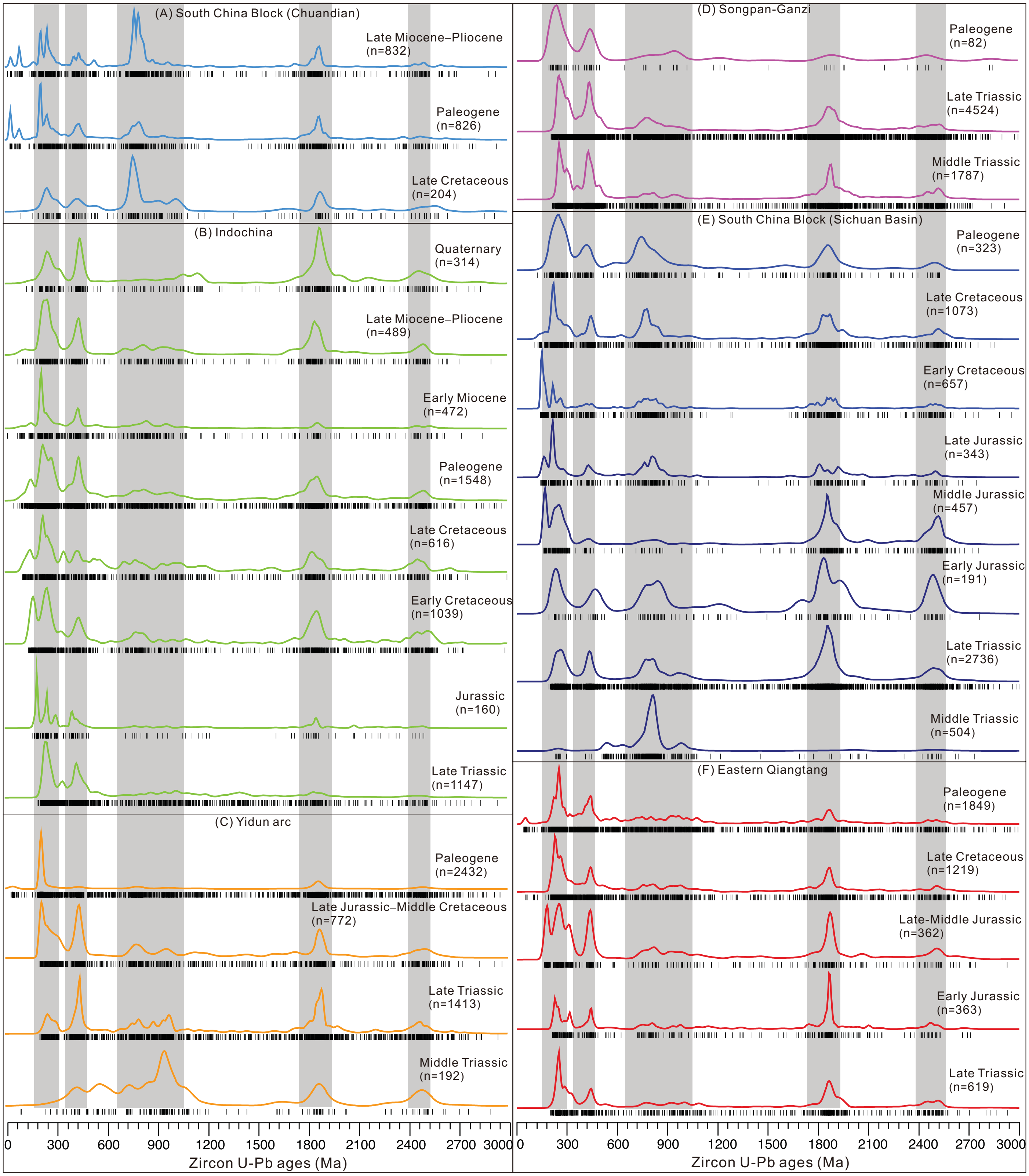
(A) South China Block (Chuandian)
Late Miocene–Pliocene (n=832)
Paleogene (n=826)
Late Cretaceous (n=204)
(B) Indochina
Quaternary (n=314)
Late Miocene–Pliocene (n=489)
Early Miocene (n=472)
Paleogene (n=1548)
Late Cretaceous (n=616)
Early Cretaceous (n=1039)
Jurassic (n=160)
Late Triassic (n=1147)
(C) Yidun arc
Paleogene (n=2432)
Late Jurassic–Middle Cretaceous (n=772)
Late Triassic (n=1413)
Middle Triassic (n=192)
(D) Songpan-Ganzi
Paleogene (n=82)
Late Triassic (n=4524)
Middle Triassic (n=1787)
(E) South China Block (Sichuan Basin)
Paleogene (n=323)
Late Cretaceous (n=1073)
Early Cretaceous (n=657)
Late Jurassic (n=343)
Middle Jurassic (n=457)
Early Jurassic (n=191)
Late Triassic (n=2736)
Middle Triassic (n=504)
(F) Eastern Qiangtang
Paleogene (n=1849)
Late Cretaceous (n=1219)
Late-Middle Jurassic (n=362)
Early Jurassic (n=363)
Late Triassic (n=619)
0 300 600 900 1200 1500 1800 2100 2400 2700 3000
Zircon U-Pb ages (Ma)

Figure 4.

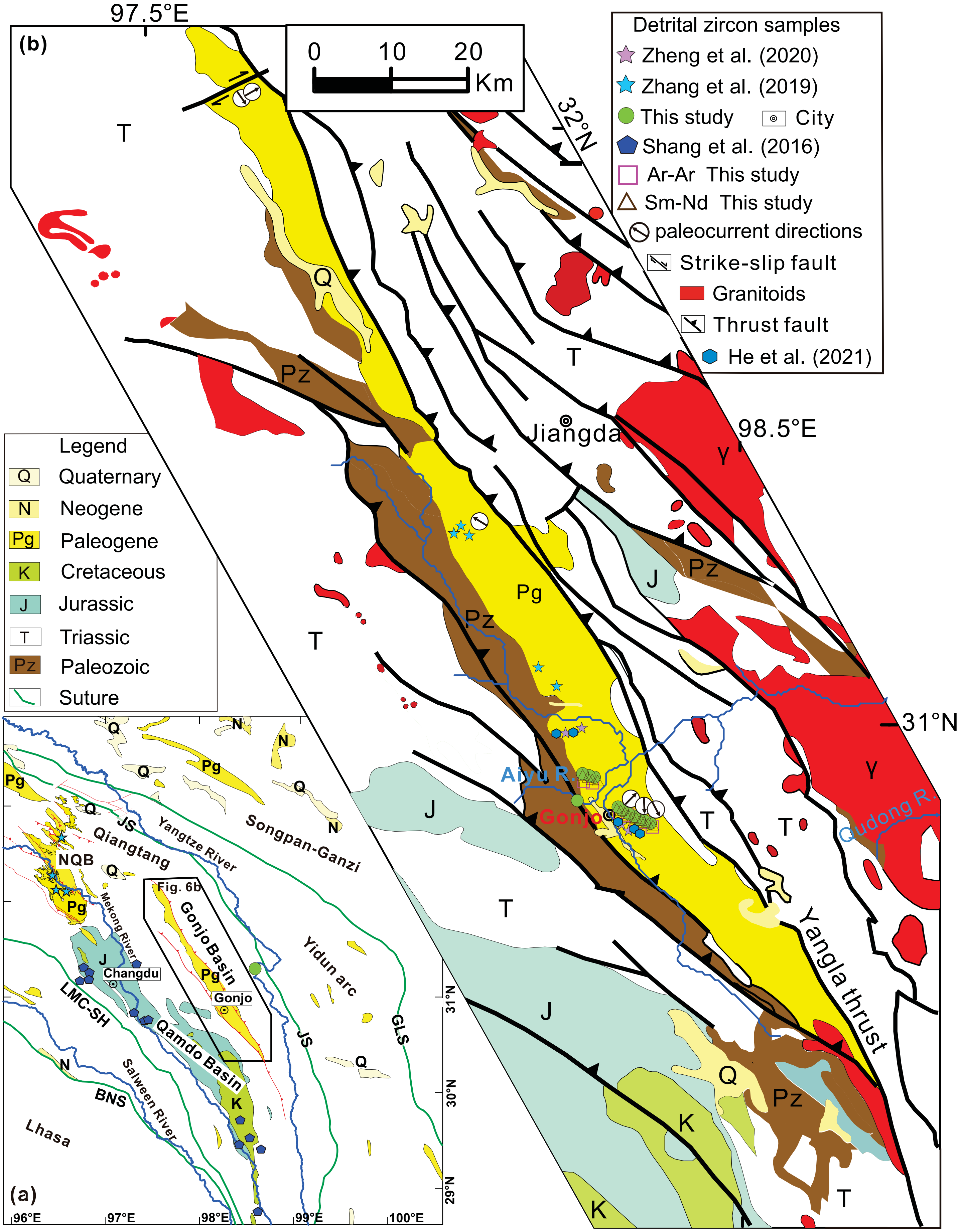

97.5°E
(b)
0 10 20 Km
32°N
Detrital zircon samples
Zheng et al. (2020)
Zhang et al. (2019)
This study
City
Shang et al. (2016)
Ar-Ar This study
Sm-Nd This study
paleocurrent directions
Strike-slip fault
Granitoids
Thrust fault
He et al. (2021)
T
Q
Pz
T
Jiangda
98.5°E
γ
Pz
J
Pg
Pz
T
31°N
Aiyu R.
Gonjo
J
T
T
γ
Qudong R.
T
Yangla thrust
J
Q
Pz
K
K
T
Legend
Q Quaternary
N Neogene
Pg Paleogene
K Cretaceous
J Jurassic
T Triassic
Pz Paleozoic
Suture
Q
N
N
Pg
Q
Pg
Q
Q
JS
Yangtze River
Songpan-Ganzi
N
Qiangtang
NQB
Q
Fig. 6b
Gonjo Basin
Mekong River
Pg
Yidun arc
J
Changdu
Pg
Gonjo
LMC-SH
Qamdo Basin
JS
GLS
N
Q
Salween River
K
BNS
Lhasa
(a)
31°N
30°N
29°N
96°E
97°E
98°E
99°E
100°E

Figure 5.

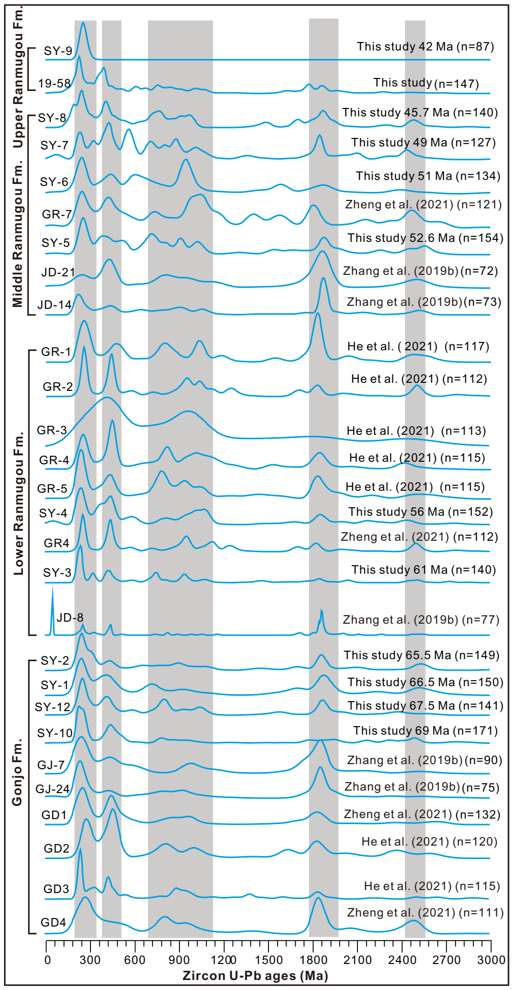

Upper Ranmugou Fm.
Middle Ranmugou Fm.
Lower Ranmugou Fm.
Gonjo Fm.
SY-9
This study 42 Ma (n=87)
19-58
This study (n=147)
SY-8
This study 45.7 Ma (n=140)
SY-7
This study 49 Ma (n=127)
SY-6
This study 51 Ma (n=134)
GR-7
Zheng et al. (2021) (n=121)
SY-5
This study 52.6 Ma (n=154)
JD-21
Zhang et al. (2019b) (n=72)
JD-14
Zhang et al. (2019b) (n=73)
GR-1
He et al. (2021) (n=117)
GR-2
He et al. (2021) (n=112)
GR-3
He et al. (2021) (n=113)
GR-4
He et al. (2021) (n=115)
GR-5
He et al. (2021) (n=115)
SY-4
This study 56 Ma (n=152)
GR4
Zheng et al. (2021) (n=112)
SY-3
This study 61 Ma (n=140)
JD-8
Zhang et al. (2019b) (n=77)
SY-2
This study 65.5 Ma (n=149)
SY-1
This study 66.5 Ma (n=150)
SY-12
This study 67.5 Ma (n=141)
SY-10
This study 69 Ma (n=171)
GJ-7
Zhang et al. (2019b) (n=90)
GJ-24
Zhang et al. (2019b) (n=75)
GD1
Zheng et al. (2021) (n=132)
GD2
He et al. (2021) (n=120)
GD3
He et al. (2021) (n=115)
GD4
Zheng et al. (2021) (n=111)
0
300
600
900
1200
1500
1800
2100
2400
2700
3000
Zircon U-Pb ages (Ma)

Figure 6.

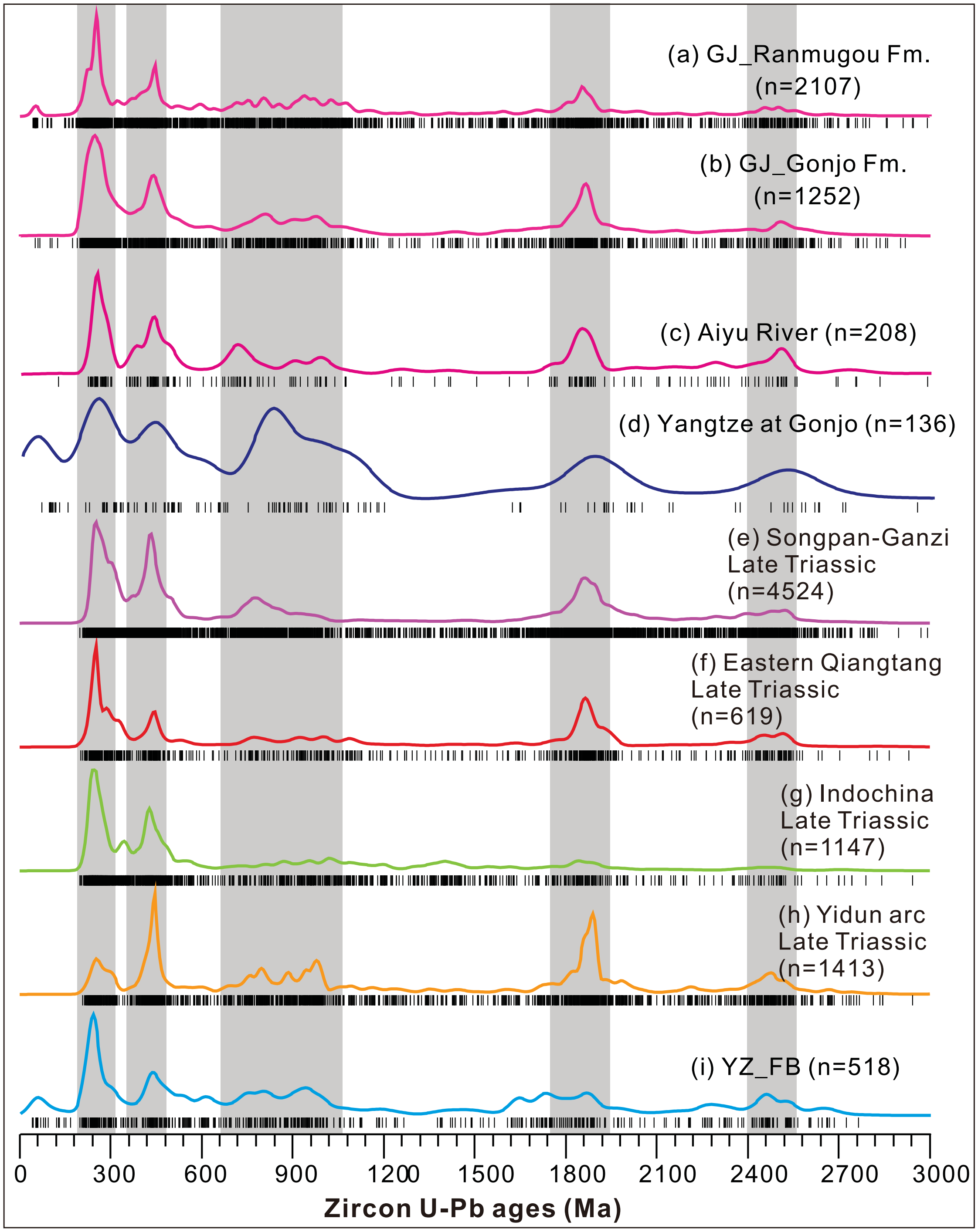
(a) GJ_Ranmugou Fm.
(n=2107)
(b) GJ_Gonjo Fm.
(n=1252)
(c) Aiyu River (n=208)
(d) Yangtze at Gonjo (n=136)
(e) Songpan-Ganzi
Late Triassic
(n=4524)
(f) Eastern Qiangtang
Late Triassic
(n=619)
(g) Indochina
Late Triassic
(n=1147)
(h) Yidun arc
Late Triassic
(n=1413)
(i) YZ_FB (n=518)
0
300
600
900
1200
1500
1800
2100
2400
2700
3000
Zircon U-Pb ages (Ma)

Figure 7.

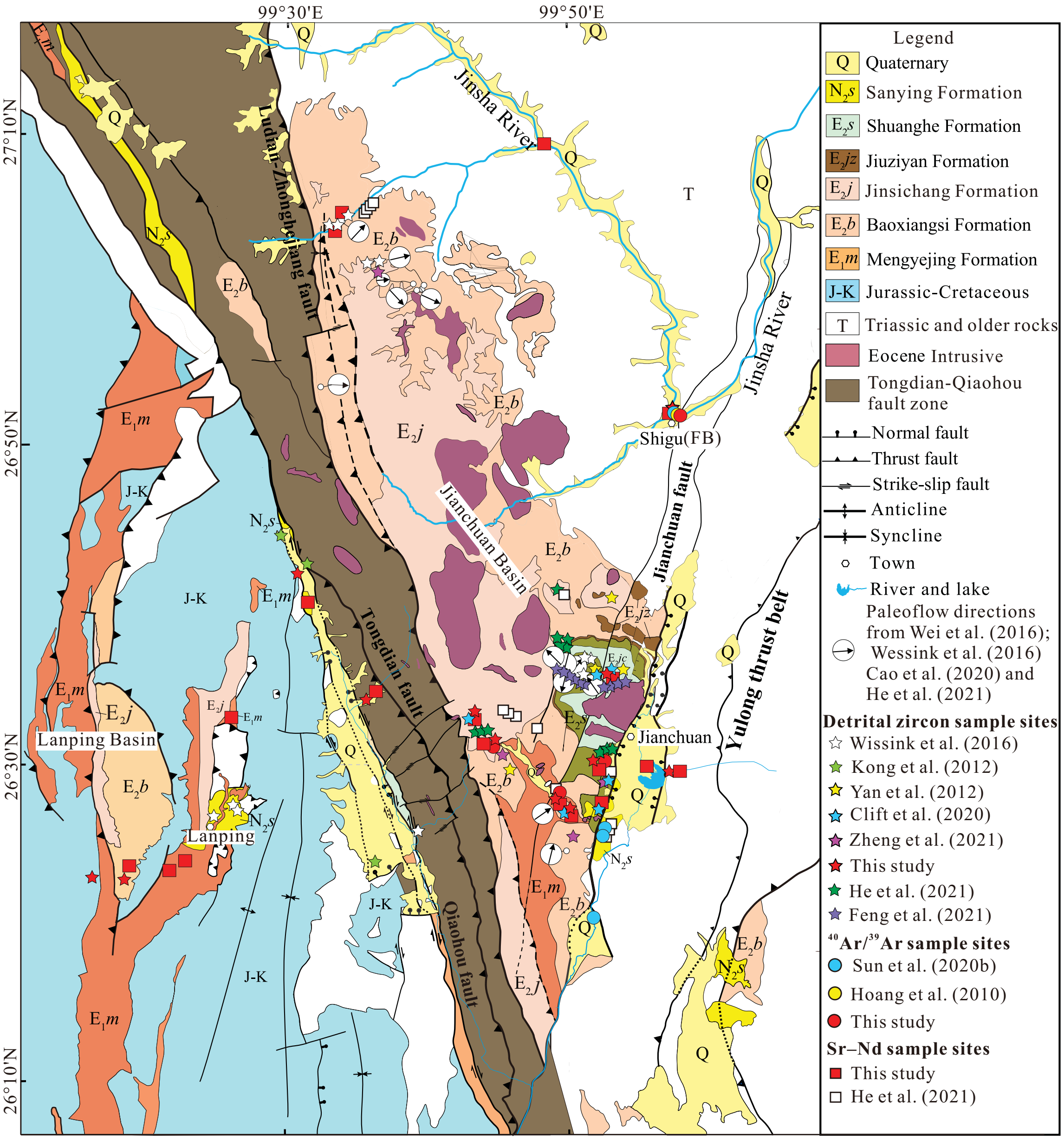

99°30'E
99°50'E
27°10'N
26°50'N
26°30'N
26°10'N
Legend
Q Quaternary
N2s Sanying Formation
E2s Shuanghe Formation
E2jz Jiuziyan Formation
E2j Jinsichang Formation
E2b Baoxiangsi Formation
E1m Mengyejing Formation
J-K Jurassic-Cretaceous
T Triassic and older rocks
Eocene Intrusive
Tongdian-Qiaohou fault zone
Normal fault
Thrust fault
Strike-slip fault
Anticline
Syncline
Town
River and lake
Paleoflow directions from Wei et al. (2016); Wessink et al. (2016) Cao et al. (2020) and He et al. (2021)
Detrital zircon sample sites
Wissink et al. (2016)
Kong et al. (2012)
Yan et al. (2012)
Clift et al. (2020)
Zheng et al. (2021)
This study
He et al. (2021)
Feng et al. (2021)
40Ar/39Ar sample sites
Sun et al. (2020b)
Hoang et al. (2010)
This study
Sr–Nd sample sites
This study
He et al. (2021)
Jinsha River
Ludian-Zhonghejiang fault
Jianchuan Basin
Shigu(FB)
Jianchuan fault
Jianchuan
Yulong thrust belt
Tongdian fault
Qiaohou fault
Lanping Basin
Lanping

Figure 8.

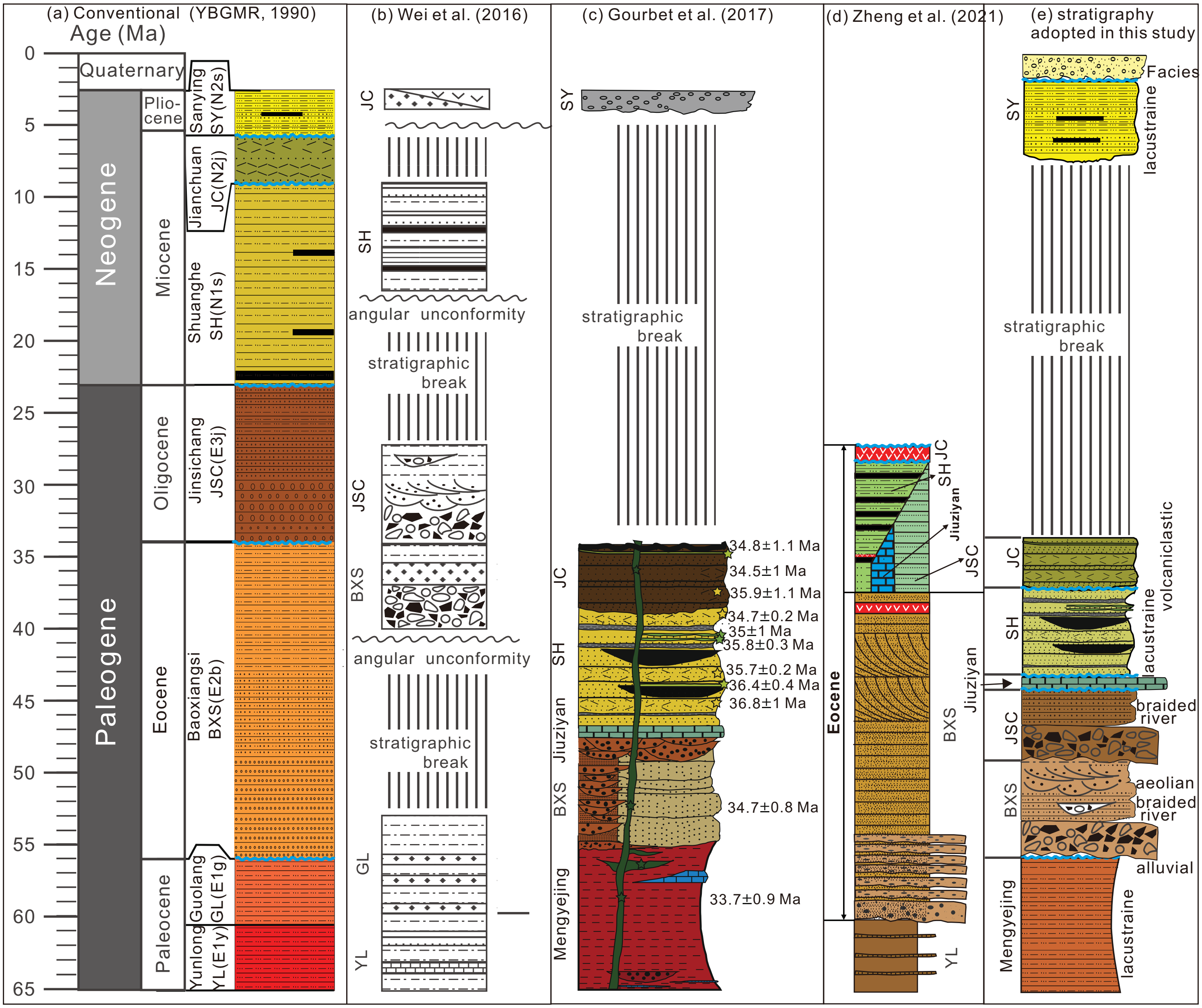
(a) Conventional (YBGMR, 1990)
Age (Ma)
0
5
10
15
20
25
30
35
40
45
50
55
60
65
Quaternary
Neogene
Paleogene
Plio-cene
Miocene
Oligocene
Eocene
Paleocene
Sanying SY(N2s)
Jianchuan JC(N2j)
Shuanghe SH(N1s)
Jinsichang JSC(E3j)
Baoxiangsi BXS(E2b)
Guolang GL(E1g)
Yunlong YL(E1y)
(b) Wei et al. (2016)
JC
SH
angular unconformity
stratigraphic break
JSC
BXS
angular unconformity
stratigraphic break
GL
YL
(c) Gourbet et al. (2017)
SY
stratigraphic break
JC
SH
Jiuziyan
BXS
Mengyejing
34.8±1.1 Ma
34.5±1 Ma
35.9±1.1 Ma
34.7±0.2 Ma
35±1 Ma
35.8±0.3 Ma
35.7±0.2 Ma
36.4±0.4 Ma
36.8±1 Ma
34.7±0.8 Ma
33.7±0.9 Ma
(d) Zheng et al. (2021)
Eocene
JC
SH
Jiuziyan
JSC
Jiuziyan
BXS
YL
(e) stratigraphy adopted in this study
Facies
SY
lacustraine
stratigraphic break
JC
volcaniclastic
SH
lacustraine
JSC
braided river
BXS
aeolian
braided river
alluvial
Mengyejing
lacustraine

Figure 9.

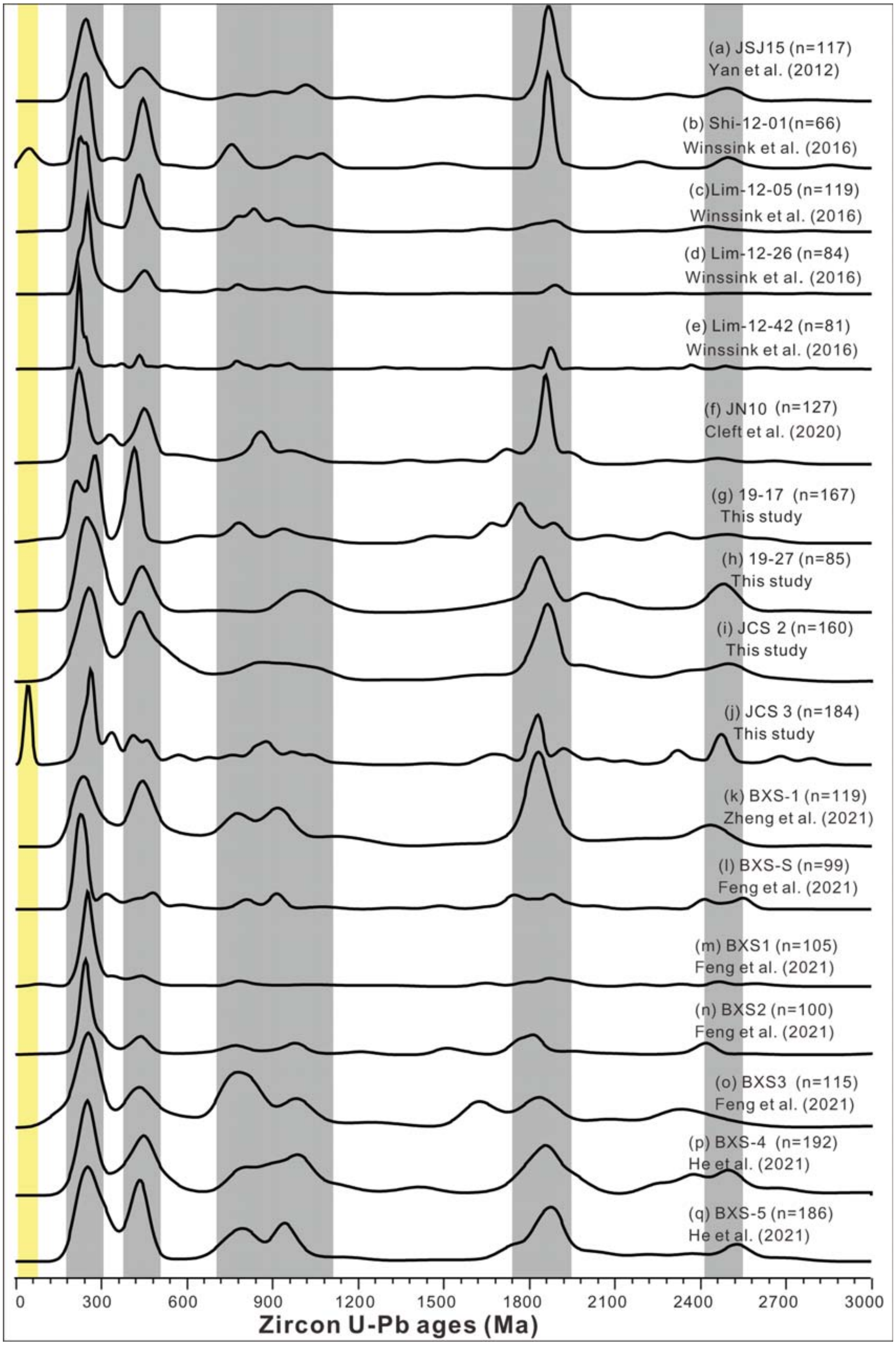
(a) JSJ15 (n=117)
Yan et al. (2012)
(b) Shi-12-01(n=66)
Winssink et al. (2016)
(c)Lim-12-05 (n=119)
Winssink et al. (2016)
(d) Lim-12-26 (n=84)
Winssink et al. (2016)
(e) Lim-12-42 (n=81)
Winssink et al. (2016)
(f) JN10 (n=127)
Cleft et al. (2020)
(g) 19-17 (n=167)
This study
(h) 19-27 (n=85)
This study
(i) JCS 2 (n=160)
This study
(j) JCS 3 (n=184)
This study
(k) BXS-1 (n=119)
Zheng et al. (2021)
(l) BXS-S (n=99)
Feng et al. (2021)
(m) BXS1 (n=105)
Feng et al. (2021)
(n) BXS2 (n=100)
Feng et al. (2021)
(o) BXS3 (n=115)
Feng et al. (2021)
(p) BXS-4 (n=192)
He et al. (2021)
(q) BXS-5 (n=186)
He et al. (2021)
0
300
600
900
1200
1500
1800
2100
2400
2700
3000
Zircon U-Pb ages (Ma)

Figure 10.

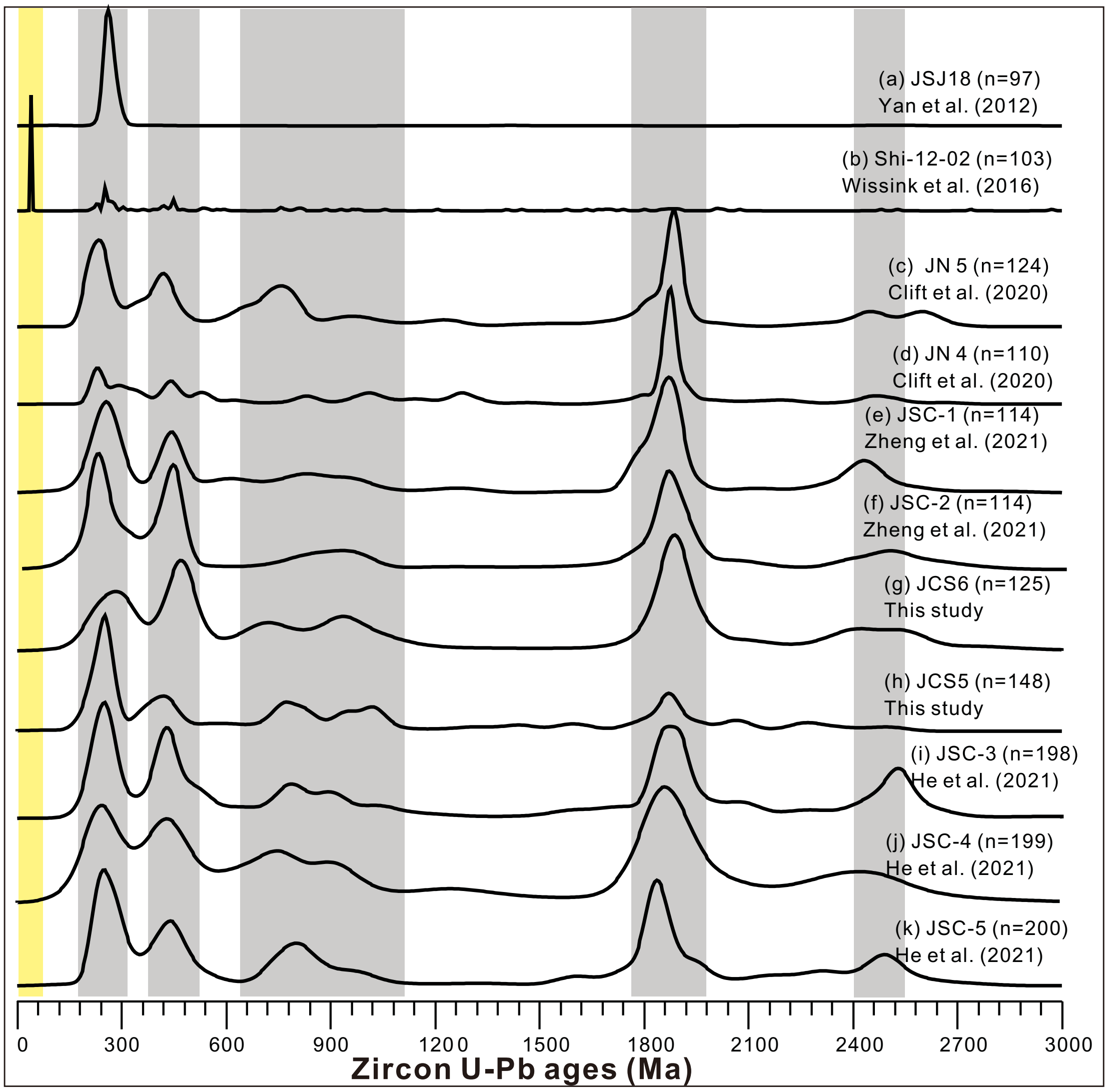
(a) JSJ18 (n=97)
Yan et al. (2012)
(b) Shi-12-02 (n=103)
Wissink et al. (2016)
(c) JN 5 (n=124)
Clift et al. (2020)
(d) JN 4 (n=110)
Clift et al. (2020)
(e) JSC-1 (n=114)
Zheng et al. (2021)
(f) JSC-2 (n=114)
Zheng et al. (2021)
(g) JCS6 (n=125)
This study
(h) JCS5 (n=148)
This study
(i) JSC-3 (n=198)
He et al. (2021)
(j) JSC-4 (n=199)
He et al. (2021)
(k) JSC-5 (n=200)
He et al. (2021)
0
300
600
900
1200
1500
1800
2100
2400
2700
3000
Zircon U-Pb ages (Ma)

Figure 11.

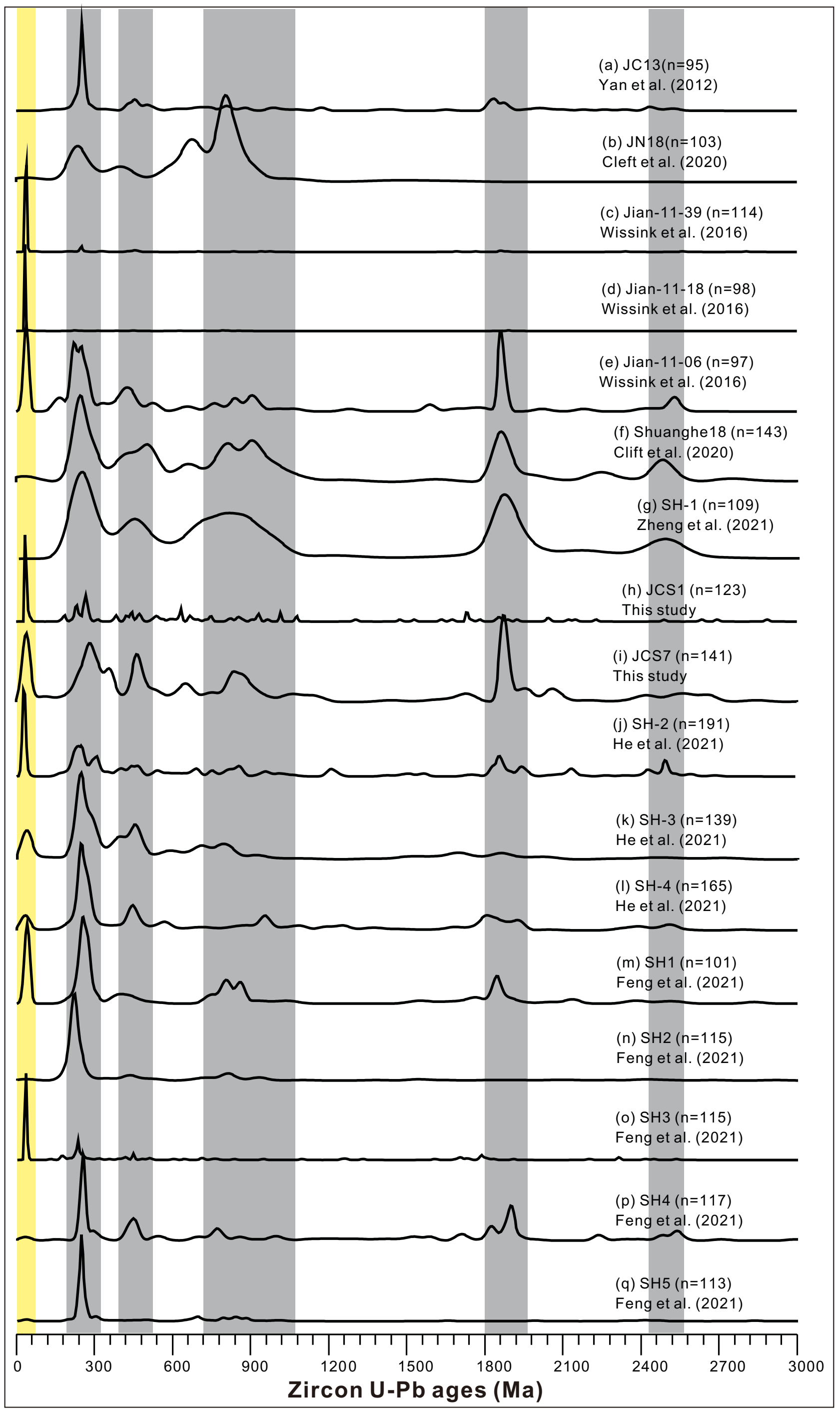

(a) JC13(n=95)
Yan et al. (2012)
(b) JN18(n=103)
Cleft et al. (2020)
(c) Jian-11-39 (n=114)
Wissink et al. (2016)
(d) Jian-11-18 (n=98)
Wissink et al. (2016)
(e) Jian-11-06 (n=97)
Wissink et al. (2016)
(f) Shuanghe18 (n=143)
Clift et al. (2020)
(g) SH-1 (n=109)
Zheng et al. (2021)
(h) JCS1 (n=123)
This study
(i) JCS7 (n=141)
This study
(j) SH-2 (n=191)
He et al. (2021)
(k) SH-3 (n=139)
He et al. (2021)
(l) SH-4 (n=165)
He et al. (2021)
(m) SH1 (n=101)
Feng et al. (2021)
(n) SH2 (n=115)
Feng et al. (2021)
(o) SH3 (n=115)
Feng et al. (2021)
(p) SH4 (n=117)
Feng et al. (2021)
(q) SH5 (n=113)
Feng et al. (2021)
0
300
600
900
1200
1500
1800
2100
2400
2700
3000
Zircon U-Pb ages (Ma)

Figure 12.

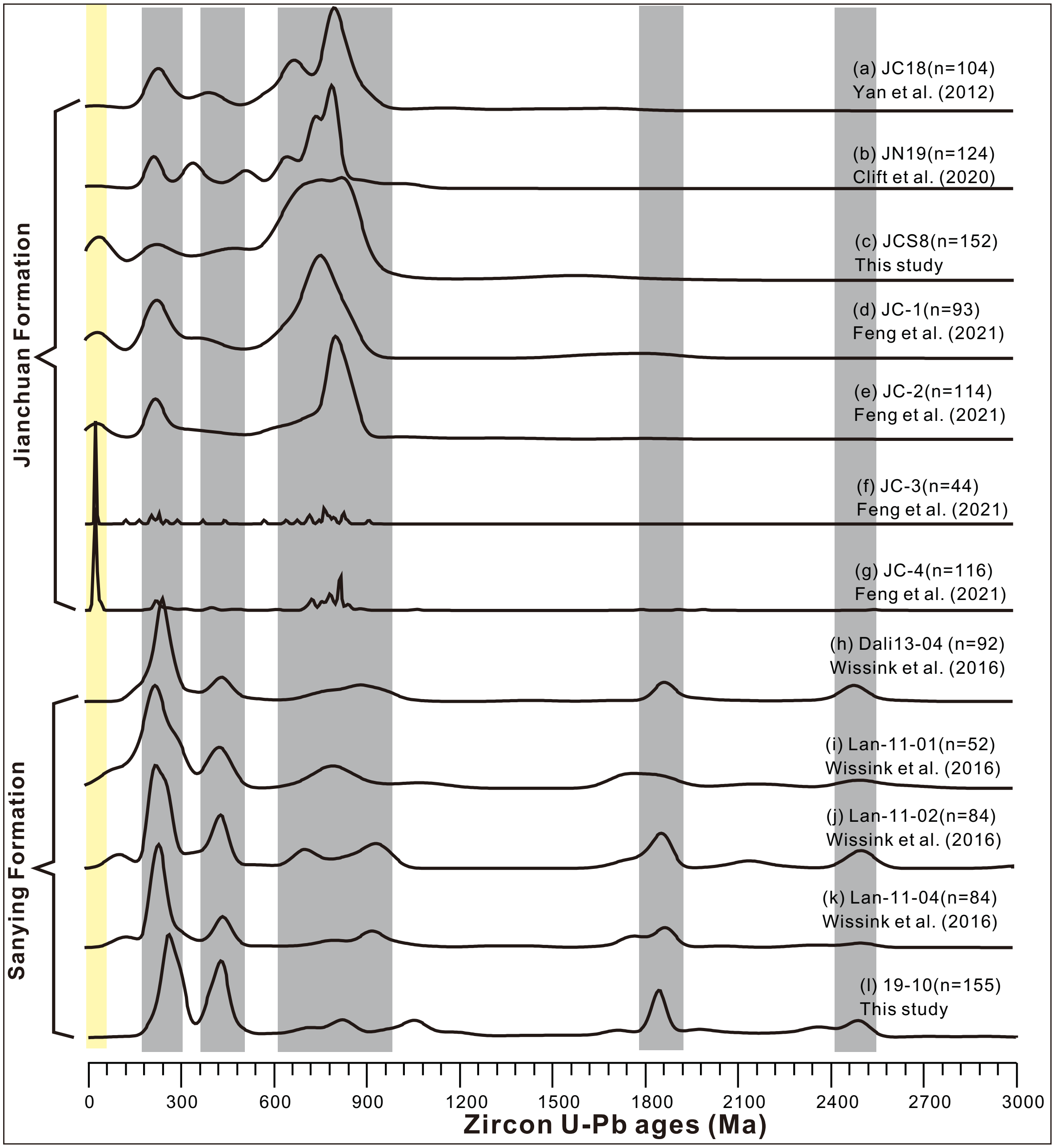
Jianchuan Formation
Sanying Formation
(a) JC18(n=104)
Yan et al. (2012)
(b) JN19(n=124)
Clift et al. (2020)
(c) JCS8(n=152)
This study
(d) JC-1(n=93)
Feng et al. (2021)
(e) JC-2(n=114)
Feng et al. (2021)
(f) JC-3(n=44)
Feng et al. (2021)
(g) JC-4(n=116)
Feng et al. (2021)
(h) Dali13-04 (n=92)
Wissink et al. (2016)
(i) Lan-11-01(n=52)
Wissink et al. (2016)
(j) Lan-11-02(n=84)
Wissink et al. (2016)
(k) Lan-11-04(n=84)
Wissink et al. (2016)
(l) 19-10(n=155)
This study
0
300
600
900
1200
1500
1800
2100
2400
2700
3000
Zircon U-Pb ages (Ma)

Figure 13.

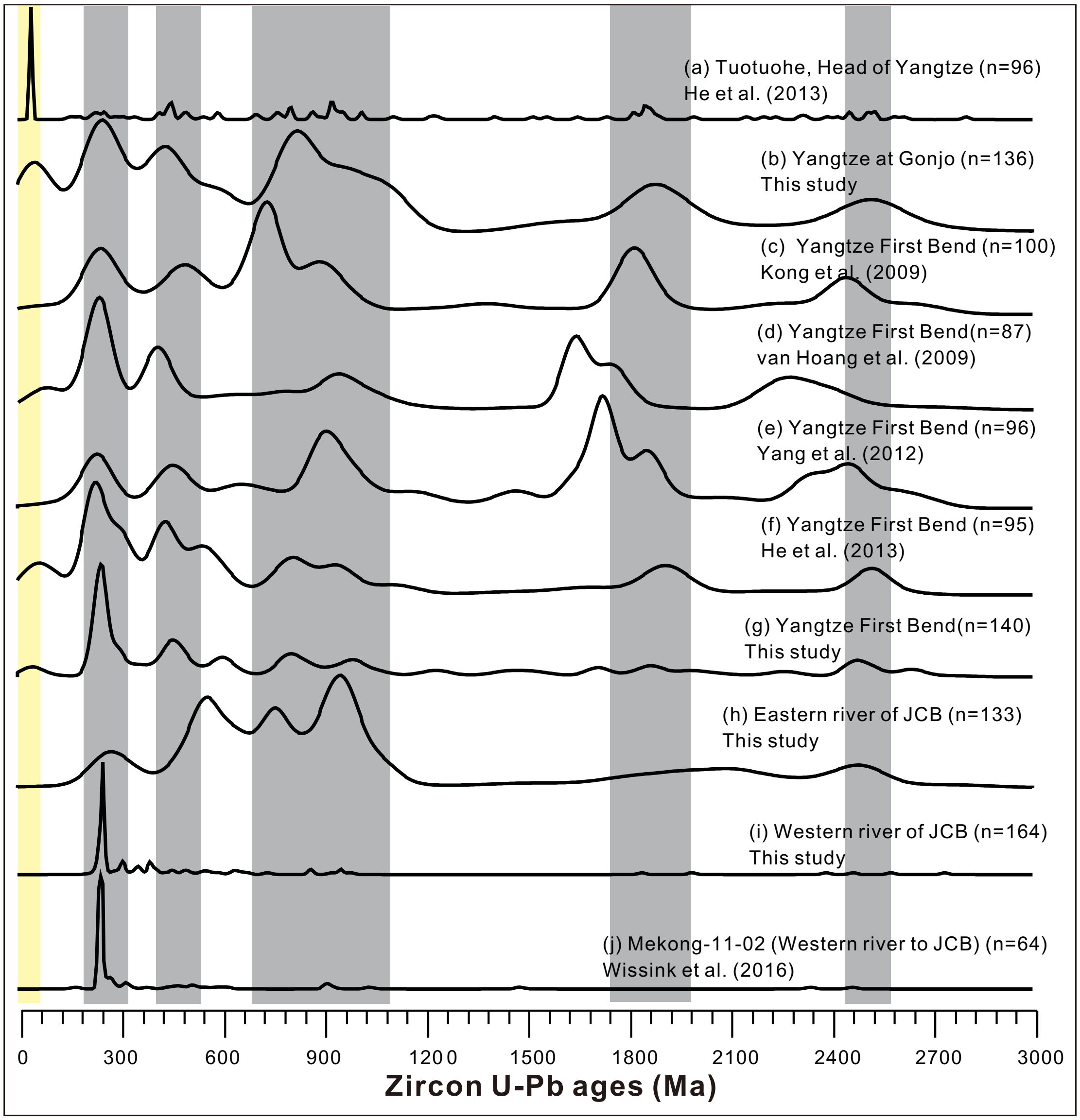

(a) Tuotuohe, Head of Yangtze (n=96)
He et al. (2013)
(b) Yangtze at Gonjo (n=136)
This study
(c) Yangtze First Bend (n=100)
Kong et al. (2009)
(d) Yangtze First Bend(n=87)
van Hoang et al. (2009)
(e) Yangtze First Bend (n=96)
Yang et al. (2012)
(f) Yangtze First Bend (n=95)
He et al. (2013)
(g) Yangtze First Bend(n=140)
This study
(h) Eastern river of JCB (n=133)
This study
(i) Western river of JCB (n=164)
This study
(j) Mekong-11-02 (Western river to JCB) (n=64)
Wissink et al. (2016)
0
300
600
900
1200
1500
1800
2100
2400
2700
3000
Zircon U-Pb ages (Ma)

Figure 14.

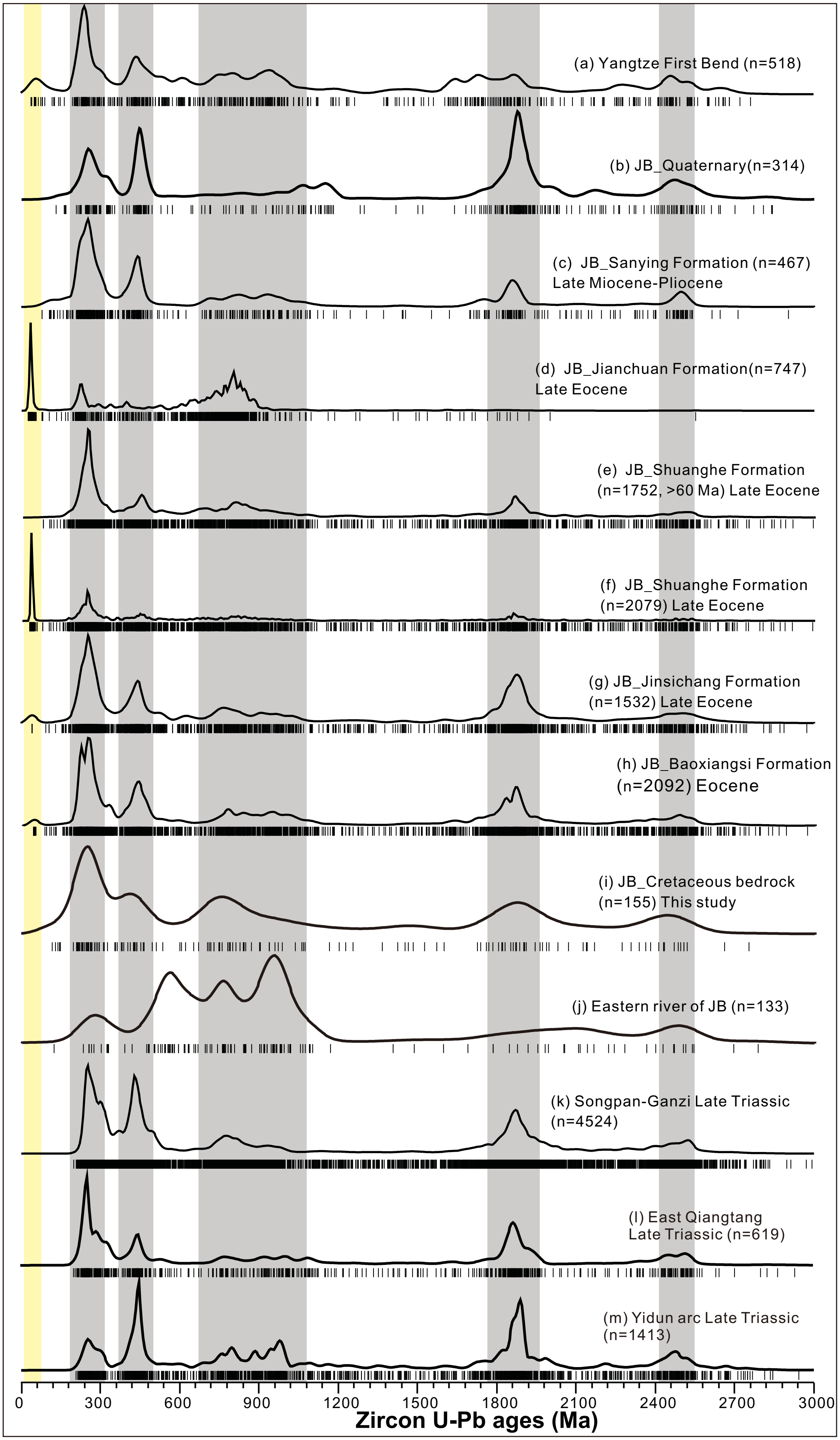

(a) Yangtze First Bend (n=518)
(b) JB_Quaternary(n=314)
(c) JB_Sanying Formation (n=467)
Late Miocene-Pliocene
(d) JB_Jianchuan Formation(n=747)
Late Eocene
(e) JB_Shuanghe Formation
(n=1752, >60 Ma) Late Eocene
(f) JB_Shuanghe Formation
(n=2079) Late Eocene
(g) JB_Jinsichang Formation
(n=1532) Late Eocene
(h) JB_Baoxiangsi Formation
(n=2092) Eocene
(i) JB_Cretaceous bedrock
(n=155) This study
(j) Eastern river of JB (n=133)
(k) Songpan-Ganzi Late Triassic
(n=4524)
(l) East Qiangtang
Late Triassic (n=619)
(m) Yidun arc Late Triassic
(n=1413)
0
300
600
900
1200
1500
1800
2100
2400
2700
3000
Zircon U-Pb ages (Ma)

Figure 15.

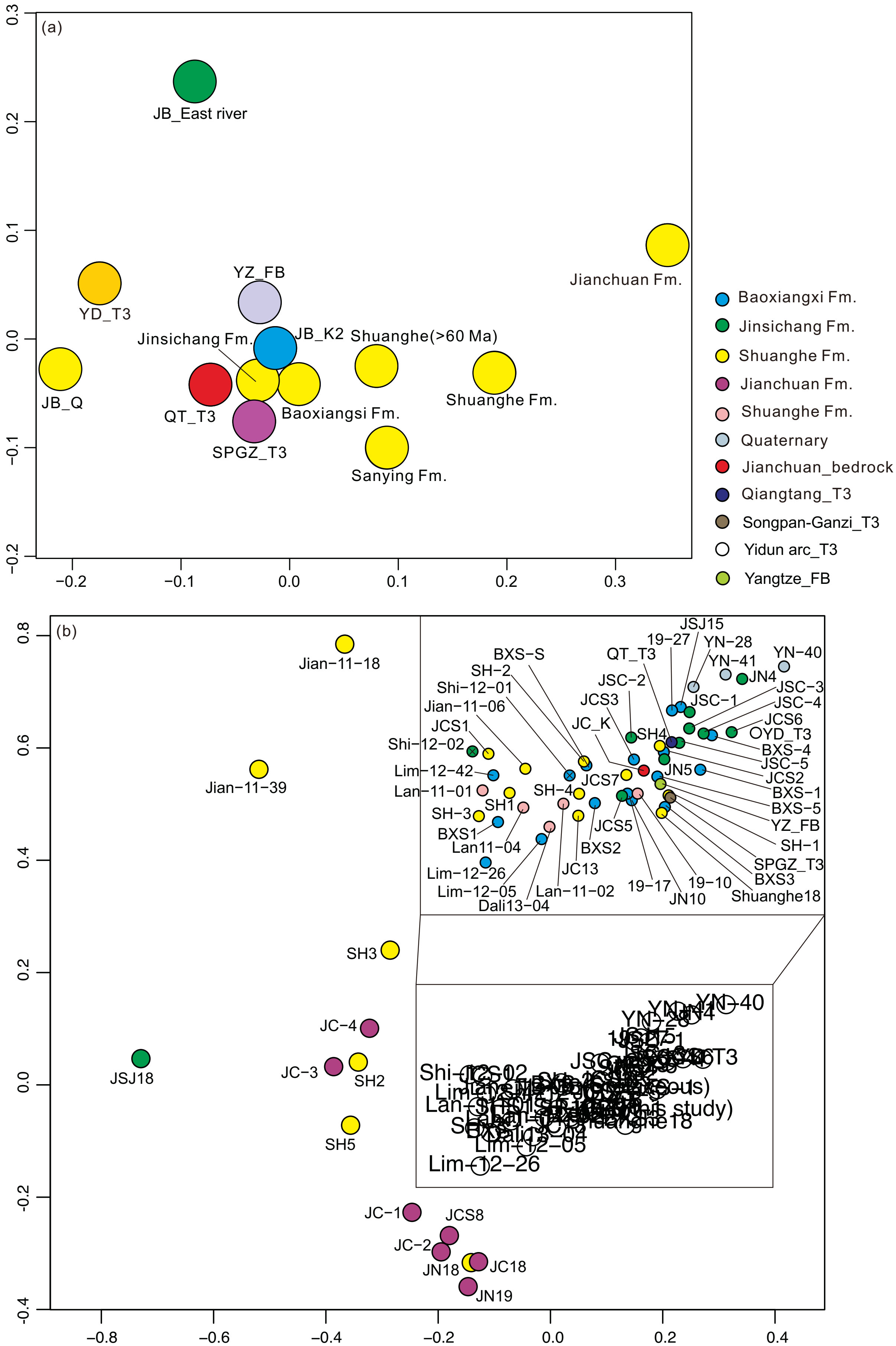

(a)
JB_East river
Jianchuan Fm.
YZ_FB
YD_T3
Jinsichang Fm.
JB_K2
Shuanghe(>60 Ma)
JB_Q
QT_T3
Baoxiangsi Fm.
Shuanghe Fm.
SPGZ_T3
Sanying Fm.
Baoxiangxi Fm.
Jinsichang Fm.
Shuanghe Fm.
Jianchuan Fm.
Shuanghe Fm.
Quaternary
Jianchuan_bedrock
Qiangtang_T3
Songpan-Ganzi_T3
Yidun arc_T3
Yangtze_FB
(b)
Jian−11−18
Jian−11−39
SH3
JC−4
JSJ18
JC−3
SH2
SH5
JC−1
JCS8
JC−2
JN18
JC18
JN19
BXS−S
SH−2
Shi−12−01
Jian−11−06
JCS1
Shi−12−02
Lim−12−42
Lan−11−01
SH1
SH−3
BXS1
Lan11−04
Lim−12−26
Lim−12−05
Dali13−04
SH−4
JCS7
JC_K
JCS3
JSC−2
QT_T3
19−27
JSJ15
YN−28
YN−41
YN−40
JN4
JSC−1
JSC−3
JSC−4
JCS6
YD_T3
SH4
BXS−4
JSC−5
JN5
JCS2
BXS−1
BXS−5
YZ_FB
SH−1
SPGZ_T3
BXS3
Shuanghe18
JCS5
BXS2
JC13
Lan−11−02
19−17
JN10
19−10
YN−40
Lim−12−05
Lim−12−26

Figure 16.

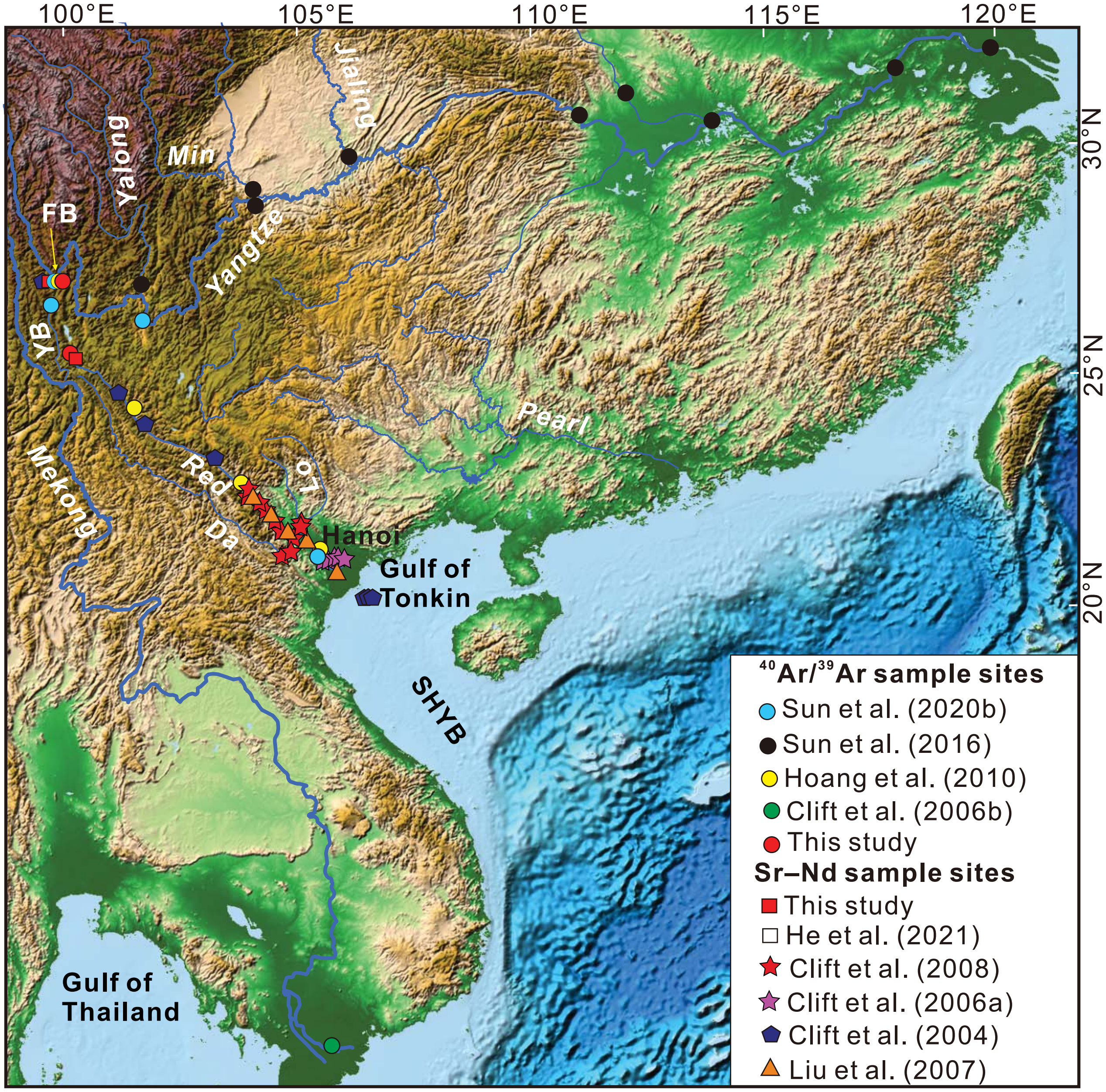

100°E
105°E
110°E
115°E
120°E
30°N
25°N
20°N
Jialing
Yalong
Min
Yangtze
FB
YB
Mekong
Red
Lo
Da
Pearl
Hanoi
Gulf of Tonkin
SHYB
Gulf of Thailand
$^{40}Ar/^{39}Ar$ sample sites
Sun et al. (2020b)
Sun et al. (2016)
Hoang et al. (2010)
Clift et al. (2006b)
This study
Sr–Nd sample sites
This study
He et al. (2021)
Clift et al. (2008)
Clift et al. (2006a)
Clift et al. (2004)
Liu et al. (2007)

Figure 17.

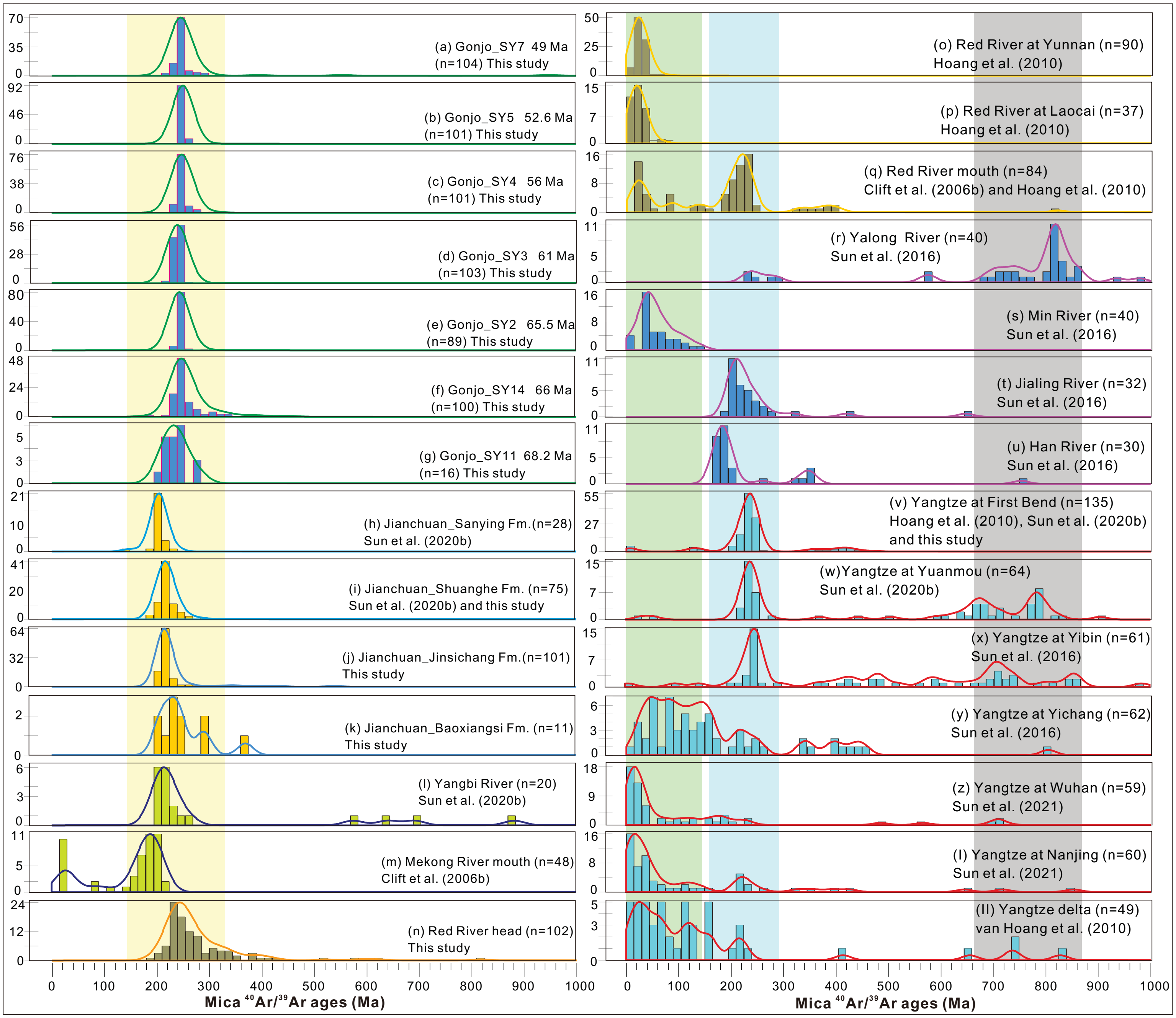

(a) Gonjo_SY7 49 Ma (n=104) This study
(b) Gonjo_SY5 52.6 Ma (n=101) This study
(c) Gonjo_SY4 56 Ma (n=101) This study
(d) Gonjo_SY3 61 Ma (n=103) This study
(e) Gonjo_SY2 65.5 Ma (n=89) This study
(f) Gonjo_SY14 66 Ma (n=100) This study
(g) Gonjo_SY11 68.2 Ma (n=16) This study
(h) Jianchuan_Sanying Fm.(n=28) Sun et al. (2020b)
(i) Jianchuan_Shuanghe Fm. (n=75) Sun et al. (2020b) and this study
(j) Jianchuan_Jinsichang Fm.(n=101) This study
(k) Jianchuan_Baoxiangsi Fm. (n=11) This study
(l) Yangbi River (n=20) Sun et al. (2020b)
(m) Mekong River mouth (n=48) Clift et al. (2006b)
(n) Red River head (n=102) This study
Mica 40Ar/39Ar ages (Ma)
(o) Red River at Yunnan (n=90) Hoang et al. (2010)
(p) Red River at Laocai (n=37) Hoang et al. (2010)
(q) Red River mouth (n=84) Clift et al. (2006b) and Hoang et al. (2010)
(r) Yalong River (n=40) Sun et al. (2016)
(s) Min River (n=40) Sun et al. (2016)
(t) Jialing River (n=32) Sun et al. (2016)
(u) Han River (n=30) Sun et al. (2016)
(v) Yangtze at First Bend (n=135) Hoang et al. (2010), Sun et al. (2020b) and this study
(w)Yangtze at Yuanmou (n=64) Sun et al. (2020b)
(x) Yangtze at Yibin (n=61) Sun et al. (2016)
(y) Yangtze at Yichang (n=62) Sun et al. (2016)
(z) Yangtze at Wuhan (n=59) Sun et al. (2021)
(I) Yangtze at Nanjing (n=60) Sun et al. (2021)
(II) Yangtze delta (n=49) van Hoang et al. (2010)
Mica 40Ar/39Ar ages (Ma)

Figure 18.

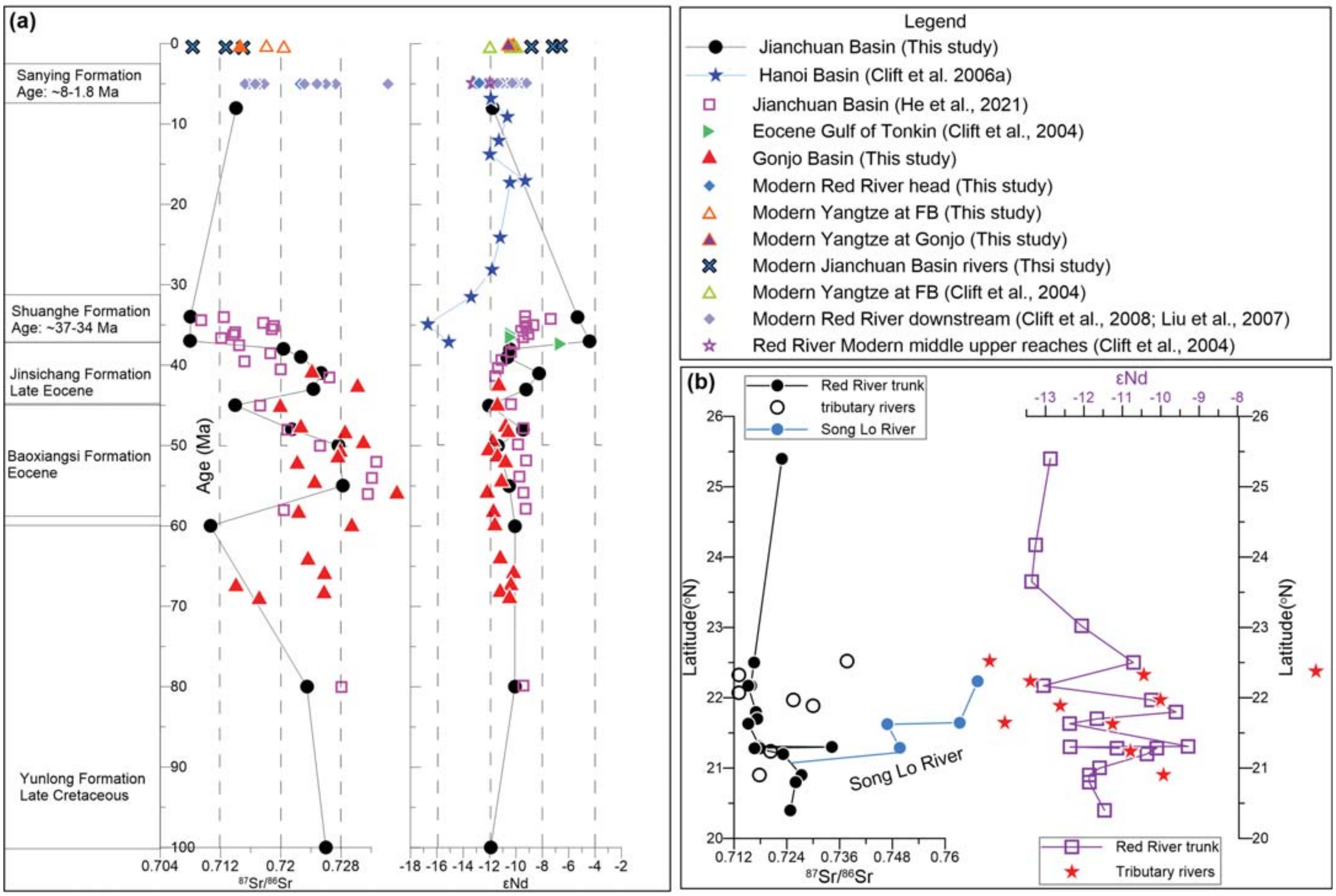
(a)
Sanying Formation
Age: ~8-1.8 Ma
Shuanghe Formation
Age: ~37-34 Ma
Jinsichang Formation
Late Eocene
Baoxiangsi Formation
Eocene
Yunlong Formation
Late Cretaceous
Age (Ma)
87Sr/86Sr
εNd
Legend
Jianchuan Basin (This study)
Hanoi Basin (Clift et al. 2006a)
Jianchuan Basin (He et al., 2021)
Eocene Gulf of Tonkin (Clift et al., 2004)
Gonjo Basin (This study)
Modern Red River head (This study)
Modern Yangtze at FB (This study)
Modern Yangtze at Gonjo (This study)
Modern Jianchuan Basin rivers (Thsi study)
Modern Yangtze at FB (Clift et al., 2004)
Modern Red River downstream (Clift et al., 2008; Liu et al., 2007)
Red River Modern middle upper reaches (Clift et al., 2004)
(b)
Red River trunk
tributary rivers
Song Lo River
Song Lo River
Latitude(°N)
87Sr/86Sr
εNd
Red River trunk
Tributary rivers

Figure 19.

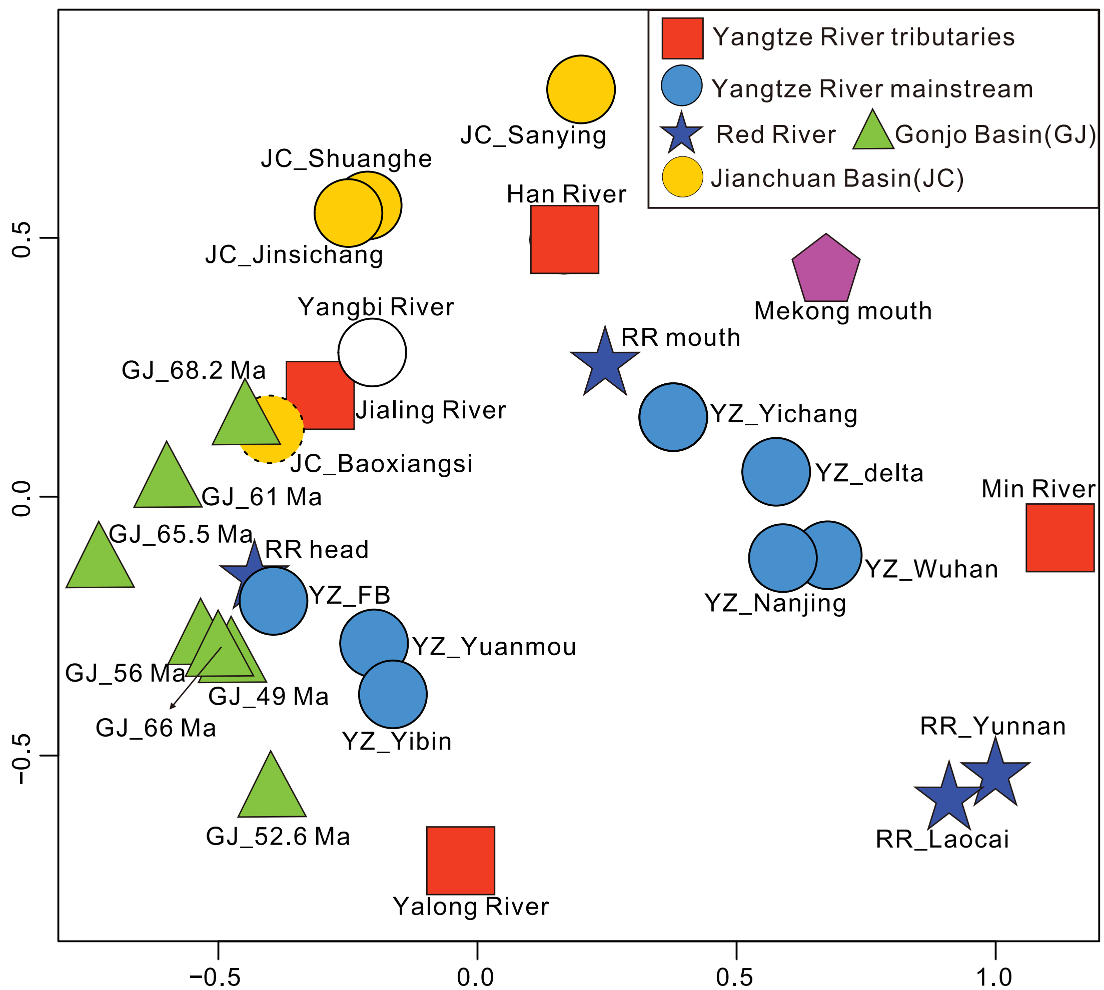
Yangtze River tributaries
Yangtze River mainstream
Red River
Gonjo Basin(GJ)
Jianchuan Basin(JC)
JC_Sanying
JC_Shuanghe
JC_Jinsichang
Han River
Mekong mouth
Yangbi River
RR mouth
GJ_68.2 Ma
Jialing River
YZ_Yichang
JC_Baoxiangsi
YZ_delta
GJ_61 Ma
Min River
GJ_65.5 Ma
RR head
YZ_FB
YZ_Wuhan
YZ_Nanjing
YZ_Yuanmou
GJ_56 Ma
GJ_49 Ma
GJ_66 Ma
YZ_Yibin
RR_Yunnan
GJ_52.6 Ma
RR_Laocai
Yalong River
0.5
0.0
−0.5
−0.5
0.0
0.5
1.0

Figure 20.

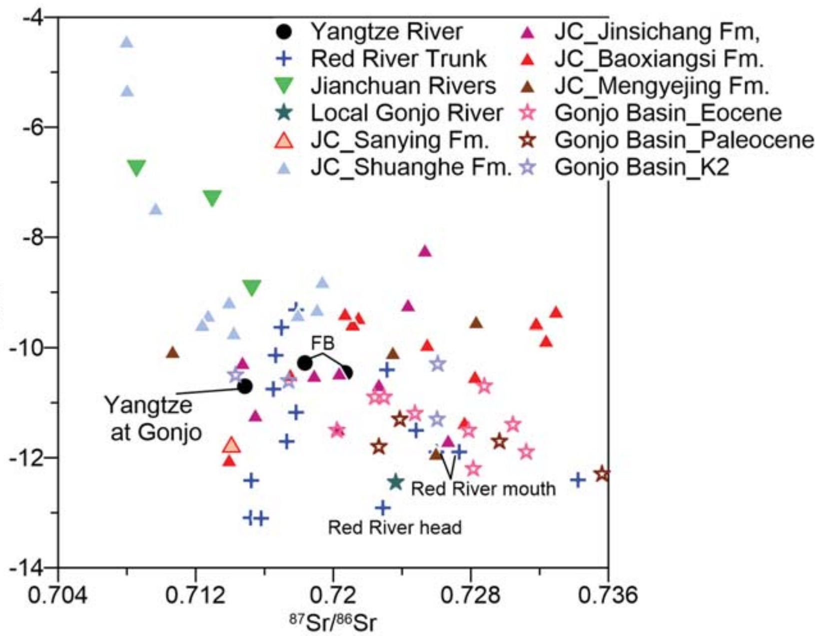
Yangtze River
Red River Trunk
Jianchuan Rivers
Local Gonjo River
JC_Sanying Fm.
JC_Shuanghe Fm.
JC_Jinsichang Fm,
JC_Baoxiangsi Fm.
JC_Mengyejing Fm.
Gonjo Basin_Eocene
Gonjo Basin_Paleocene
Gonjo Basin_K2
FB
Yangtze at Gonjo
Red River mouth
Red River head
εNd
-4
-6
-8
-10
-12
-14
0.704
0.712
0.72
0.728
0.736
87Sr/86Sr